

Contents of this file

1. Samples	4
1.1 Headwall samples	4
1.2 Englacial samples.....	4
2. Cosmogenic nuclide dating.....	10
3. Luminescence measurements.....	10
3.1 Sample preparation	10
3.2 Luminescence measurements.....	11
3.3 Environmental dose rate determination	12
3.4 Luminescence rock surface exposure dating results	12
3.4.1 Inverting for erosion rates	14
3.5 Luminescence rock surface burial dating results	25
References.....	51

Tables

Table S 1: Coordinates of the headwall samples.....	4
Table S 2: Coordinates, and sample size of the dated englacial samples.....	4
Table S 3: Single Aliquot Regenerative (SAR) protocol.....	11
Table S 4: Luminescence bleaching parameters for the headwall samples.....	13
Table S 5: Luminescence RSED results.....	14
Table S 6: Measured variables for total environmental dose rate (\dot{D}) determination.....	43
Table S 7: Dose rates, D_e values, luminescence ages calculated per rock fragment for $IRSL_{50}$	44
Table S 8: Dose rates, D_e values, luminescence ages calculated per rock fragment for $IRSL_{225}$	47

Figures

Figure S 1: Images of englacial clast samples	5
Figure S 2: Images of discs taken from cores of each of the englacial samples analysed. Each disc has a diameter of 16-18 mm.	8
Figure S 3: Calibration depth profiles and fitting parameters for the different signals A) $IRSL_{50}$, B) $IRSL_{225}$, C) OSL_{125} . Colours indicate different cores and shapes different samples. Cores 03B and 04B ($IRSL_{50}$ only) do not extend to the saturated part of the profile and have been excluded.	13
Figure S 4: Inversion results for the $IRSL_{50}$ signal of sample MDG-HF-01	15
Figure S 5: Inversion results for the $IRSL_{225}$ signal of sample MDG-HF-01	16
Figure S 6: Inversion results for the OSL_{125} signal of sample MDG-HF-01	17
Figure S 7: Inversion results for the $IRSL_{50}$ signal of sample MDG-HF-02	18
Figure S 8: Inversion results for the $IRSL_{225}$ signal of sample MDG-HF-02	18
Figure S 9: Inversion results for the OSL_{125} signal of sample MDG-HF-02	18
Figure S 10: Inversion results for the $IRSL_{50}$ signal of sample MDG-HF-03.....	19
Figure S 11: Inversion results for the $IRSL_{225}$ signal of sample MDG-HF-03	20
Figure S 12: Inversion results for the OSL_{125} signal of sample MDG-HF-03	21
Figure S 13: Inversion results for the $IRSL_{50}$ signal of sample MDG-HF-04.....	22
Figure S 14: Inversion results for the $IRSL_{225}$ signal of sample MDG-HF-04	23
Figure S 15: Inversion results for the OSL_{125} signal of sample MDG-HF-04	24
Figure S 16: Luminescence bleaching profile for the $IRSL_{50}$ signal of sample MDG23 (core 10-B2) (A) and the corresponding SAR dose response curves (B) measured for fragments on the bleaching plateau.....	25
Figure S 17: Luminescence bleaching profiles of RSBD samples: MDG23-01 (A2,B1), 02 (A2), 03 (A1).....	27
Figure S 18: Luminescence bleaching profiles of RSBD samples: MDG23-03 (A2), 04 (A1,B1), 05 (A1).....	28
Figure S 19: Luminescence bleaching profiles of RSBD samples: MDG23-06 (A1), 07 (A1,B1,C1).	29
Figure S 20: Luminescence bleaching profiles of RSBD samples: MDG23-07 (D1), 08 (A1,C1), 09 (A1).....	30
Figure S 21: Luminescence bleaching profiles of RSBD samples: MDG23-10 (A2,B2), MDG-01 (A), 02 (A).	31
Figure S 22: Luminescence bleaching profiles of RSBD samples: MDG-02 (B1), 03 (B), 06 (A), 07 (A).	32
Figure S 23: Luminescence bleaching profiles of RSBD samples: MDG-09 (A), 10 (A), 13 (A), 16(A).....	33
Figure S 24: Luminescence bleaching profiles of RSBD samples: MDG-18 (A), 19 (A), 20 (A,B).....	34
Figure S 25: Luminescence bleaching profiles of RSBD samples: MDG-21 (A), 32 (A), 33 (B).	35

Figure S 26: Dose response curve from sample MDG23_01 core A2 IRSL ₅₀ (A), IRSL ₂₂₅ (B), and core B2 IRSL ₅₀ (C), IRSL ₂₂₅ (D).....	36
Figure S 27: Dose response curve from sample MDG23_04 core A1 IRSL ₅₀ (A), IRSL ₂₂₅ (B), and core B1 IRSL ₅₀ (C), IRSL ₂₂₅ (D).....	37
Figure S 28: Dose response curve from sample MDG23_06 core A1 IRSL ₅₀	37
Figure S 29: Dose response curve from sample MDG23_07 core A1 IRSL ₅₀ (A), core C1 IRSL ₅₀ (B), and core D1 IRSL ₅₀ (C).....	38
Figure S 30: Dose response curve from sample MDG23_08 core C1 IRSL ₅₀	38
Figure S 31: Dose response curve from sample MDG23_10 core A2 IRSL ₅₀ (A), IRSL ₂₂₅ (B), and core B2 IRSL ₅₀ (C), IRSL ₂₂₅ (D).....	39
Figure S 32: Dose response curve from sample MDG_01 core A IRSL ₅₀	39
Figure S 33: Dose response curve from sample MDG_02 core B1 IRSL ₅₀	40
Figure S 34: Dose response curve from sample MDG_06 core A IRSL ₅₀	40
Figure S 35: Dose response curve from sample MDG_07 core A IRSL ₅₀	40
Figure S 36: Dose response curve from sample MDG_09 core A IRSL ₅₀	41
Figure S 37: Dose response curve from sample MDG_16 core A IRSL ₅₀ (A), IRSL ₂₂₅ (B).....	41
Figure S 38: Dose response curve from sample MDG_19 core A IRSL ₅₀	41
Figure S 39: Dose response curve from sample MDG_20 core A IRSL ₅₀ (A), core B IRSL ₅₀ (B).....	42
Figure S 40: Dose response curve from sample MDG_33 core A IRSL ₅₀	42
Figure S 41: Dose-recovery ratio, residual-subtracted dose-recovery ratio, residual doses and fading rates.....	48
Figure S 42: IRSL ₅₀ and IRSL ₂₂₅ ages and residuals.....	49
Figure S 43: IRSL ₅₀ age variability.....	49
Figure S 44: Distribution of IRSL ₅₀ ages by number of rock slice fragments in the plateau.....	50
Figure S 45: Ages from the glacier front classified by ice structure.....	50

Other tables provided as separate file

Erosion rate

Table S9. Cosmogenic nuclide (¹⁰ Be) data
Table S10. Lx/Tx measurement - MDG-HF-01 – Core 1 – Unknown age sample
Table S11. Lx/Tx measurement - MDG-HF-01 – Core 2 – Unknown age sample
Table S12. Lx/Tx measurement - MDG-HF-01 – Core A – Calibration sample of 1year
Table S13. Lx/Tx measurement - MDG-HF-01 – Core B – Calibration sample of 1year
Table S14. Lx/Tx measurement - MDG-HF-02 – Core 1 – Unknown age sample
Table S15. Lx/Tx measurement - MDG-HF-02 – Core 2 – Unknown age sample
Table S16. Lx/Tx measurement - MDG-HF-02 – Core A – Calibration sample of 1year
Table S17. Lx/Tx measurement - MDG-HF-02 – Core B – Calibration sample of 1year
Table S18. Lx/Tx measurement - MDG-HF-03 – Core 1 – Unknown age sample
Table S19. Lx/Tx measurement - MDG-HF-03 – Core 2 – Unknown age sample
Table S20. Lx/Tx measurement - MDG-HF-03 – Core A – Calibration sample of 1year
Table S21. Lx/Tx measurement - MDG-HF-04 – Core 1 – Unknown age sample
Table S22. Lx/Tx measurement - MDG-HF-04 – Core 2 – Unknown age sample
Table S23. Lx/Tx measurement - MDG-HF-04 – Core A – Calibration sample of 1year
Table S24. Lx/Tx measurement - MDG-HF-04 – Core B – Calibration sample of 1year
Table S25. IRSL ₅₀ bootstrapping results
Table S26. IRSL ₂₂₅ bootstrapping results
Table S27. OSL ₁₂₅ bootstrapping results
Table S28. Erosion rates inverted from TCN and RSED

Englacial transport

Table S29. Coordinates, sample dimensions, samples and location description
Table S30. Ice structure and ice cover information per sample
Table S31. Lx/Tx measurement - MDG23-01 – Core A2
Table S32. Lx/Tx measurement - MDG23-01 – Core B1
Table S33. Lx/Tx measurement - MDG23-02 – Core A2
Table S34. Lx/Tx measurement - MDG23-03 – Core A1
Table S35. Lx/Tx measurement - MDG23-03 – Core A2
Table S36. Lx/Tx measurement - MDG23-04 – Core A1

Table S37. Lx/Tx measurement - MDG23-04 – Core A2
 Table S38. Lx/Tx measurement - MDG23-05A – Core A1
 Table S39. Lx/Tx measurement - MDG23-06 – Core A1
 Table S40. Lx/Tx measurement - MDG23-07 – Core A1
 Table S41. Lx/Tx measurement - MDG23-07 – Core B1
 Table S42. Lx/Tx measurement - MDG23-07 – Core C1
 Table S43. Lx/Tx measurement - MDG23-07 – Core D1
 Table S44. Lx/Tx measurement - MDG23-08 – Core A1
 Table S45. Lx/Tx measurement - MDG23-08 – Core C1
 Table S46. Lx/Tx measurement - MDG23-09 – Core A1
 Table S47. Lx/Tx measurement - MDG23-10 – Core A2
 Table S48. Lx/Tx measurement - MDG23-10 – Core B2
 Table S49. Lx/Tx measurement - MDG-01 – Core A
 Table S50. Lx/Tx measurement - MDG-02 – Core A
 Table S51. Lx/Tx measurement - MDG-02 – Core B1
 Table S52. Lx/Tx measurement - MDG-03 – Core B
 Table S53. Lx/Tx measurement - MDG-04 – Core A
 Table S54. Lx/Tx measurement - MDG-06 – Core A
 Table S55. Lx/Tx measurement - MDG-07 – Core A
 Table S56. Lx/Tx measurement - MDG-09 – Core A
 Table S57. Lx/Tx measurement - MDG-10 – Core A
 Table S58. Lx/Tx measurement - MDG-13 – Core A
 Table S59. Lx/Tx measurement - MDG-14 – Core A
 Table S60. Lx/Tx measurement - MDG-16 – Core A
 Table S61. Lx/Tx measurement - MDG-18 – Core A
 Table S62. Lx/Tx measurement - MDG-19 – Core A
 Table S63. Lx/Tx measurement - MDG-20 – Core A
 Table S64. Lx/Tx measurement - MDG-20 – Core B
 Table S65. Lx/Tx measurement - MDG-21 – Core B
 Table S66. Lx/Tx measurement - MDG-23 – Core A
 Table S67. Lx/Tx measurement - MDG-32 – Core A
 Table S68. Lx/Tx measurement - MDG-33 – Core A
 Table S69. Sample preparation details – slicing and coring
 Table S70. Calc_CobbleDoseRate – Input & output
 Table S71. DRAC - Input & output
 Table S72. DRR, residual and RSDRR per sample for IRSL₅₀, IRSL₂₂₅, OSL₁₂₅
 Table S73: Selected (in bold) and rejected cores for dating.
 Table S74: IRSL₅₀, IRSL₂₂₅ and OSL₁₂₅ luminescence success for selected core to date

1. Samples

1.1 Headwall samples

Table S 1: Coordinates of the headwall samples

Sample name	Latitude (dd)	Longitude (dd)	Elevation (m)
MDG-HF-01	45.84986	6.92798	3219
MDG-HF-02	45.85013	6.9282	3219
MDG-HF-03	45.85035	6.92828	3219
MDG-HF-04	45.85013	6.92811	3416

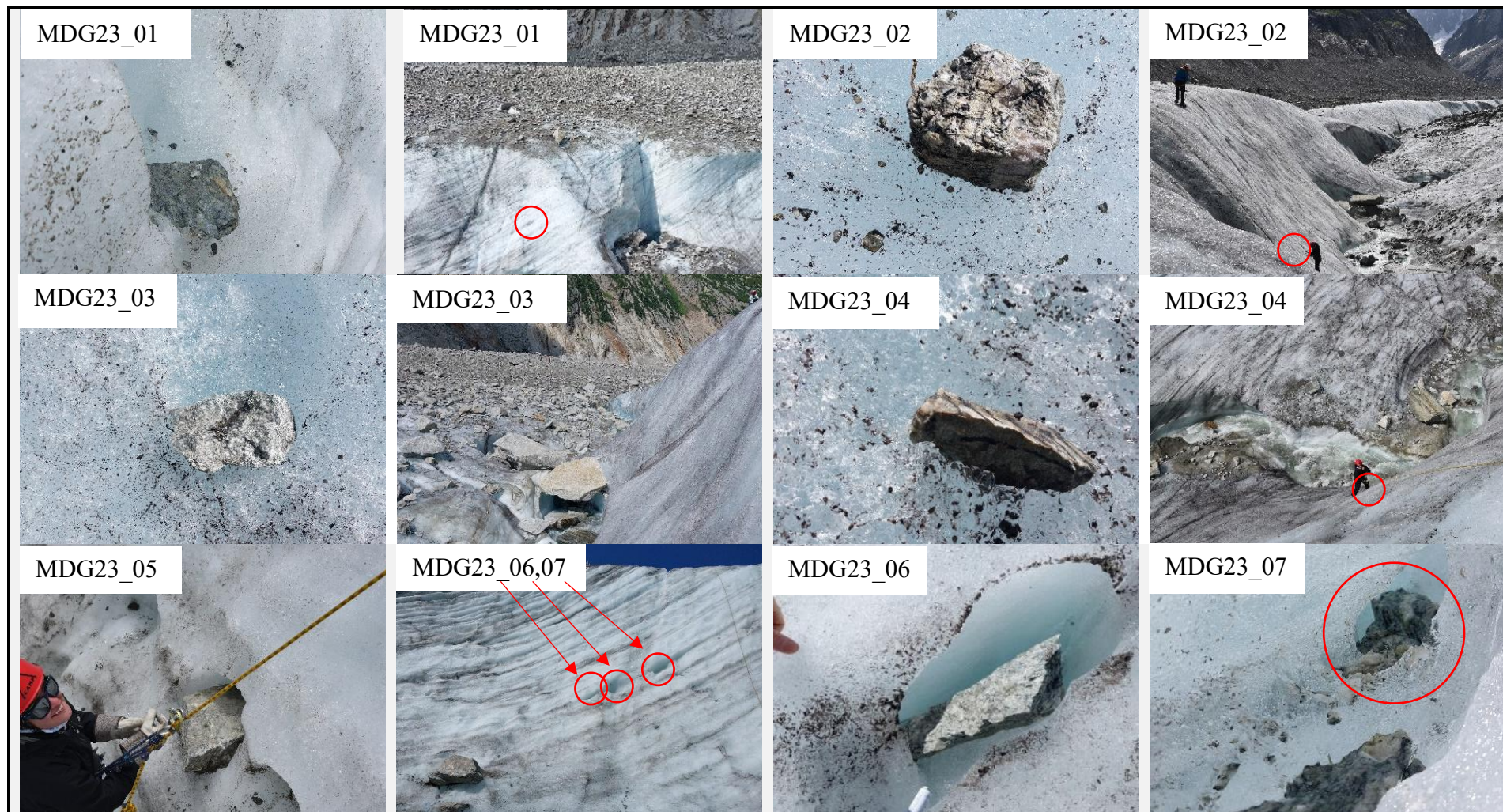
1.2 Englacial samples

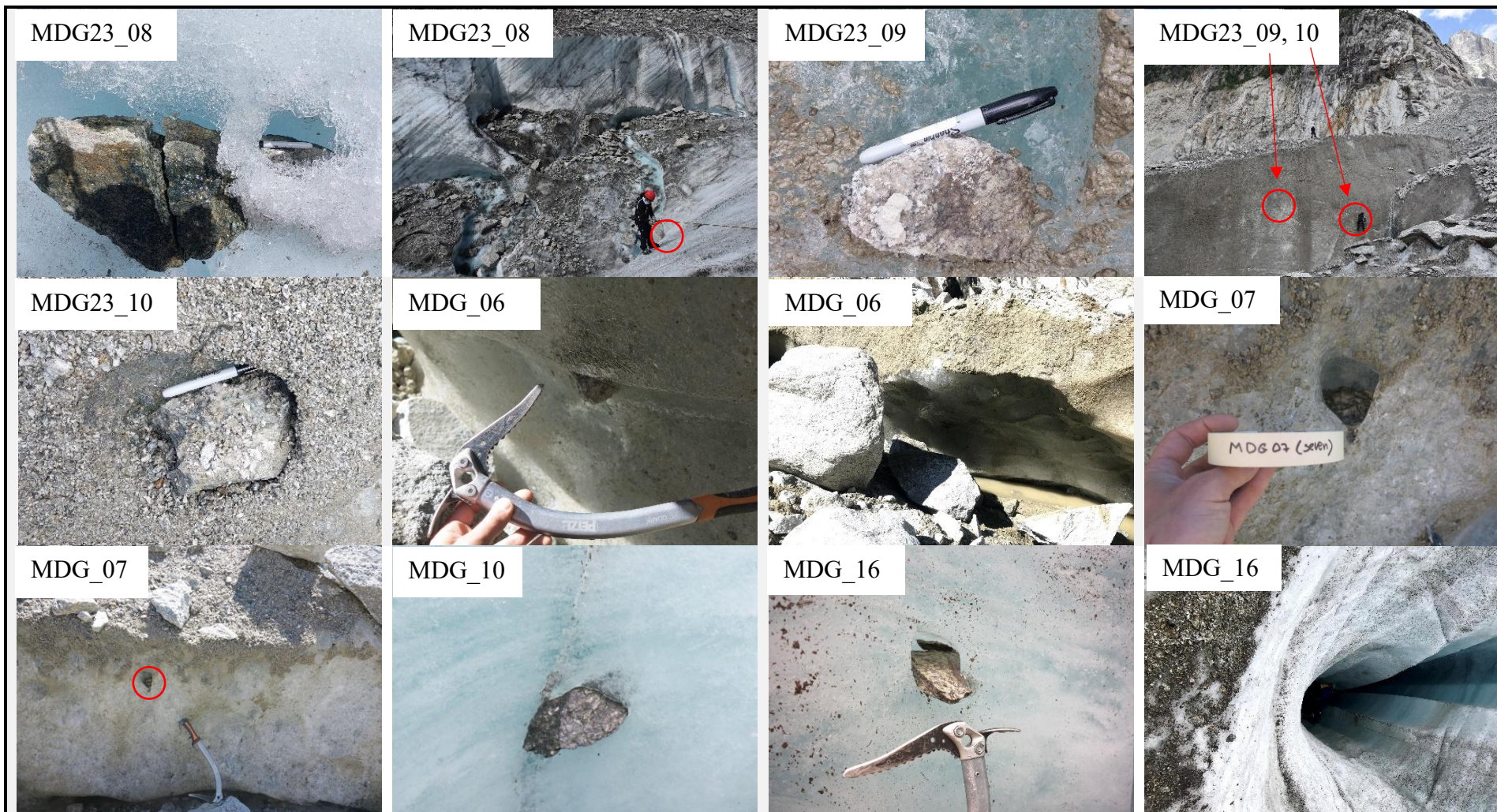
Table S 2: Coordinates, and sample size of the dated englacial samples

Note that the location description and field information can be found in Table S29.

Sample name	Latitude [dd]	Longitude [dd]	Altitude ¹ [m a.s.l]	Depth into ice [m]	Distance from the Glacier front [m]	Dimension [cm]
MDG23_01	45.9143	6.937639	2018	7.1	2900±50	16x12x6
MDG23_04	45.9159194	6.9358083	1958	6.1	2700±50	13x5x4
MDG23_06	45.914306	6.937639	1894	4.3	2880±50	14x7x4
MDG23_07	45.914306	6.937639	1894	4.4	2880±50	27x20x8
MDG23_08	45.9153056	6.9373611	1884	10.4	2810±50	22x14x12
MDG23_10	45.9232667	6.9247167	1693	9	1520±50	25x14x7
MDG_01	45.92506	6.92304	1696	2	1200±50	10x7x5.5
MDG_02	45.92506	6.92304	1696	2	1200±50	22x17x7
MDG_06	45.93016	6.92509	1646	ND	700±50	30x20x17
MDG_07	45.93008	6.92444	1640	-1	750±50	19x14x6
MDG_09	45.92949	6.92429	ND	18	900±50	8x6x3
MDG_16	45.92131	6.92591	1777	8	1860±50	18x12x4.5
MDG_19	45.92	6.92641	1818	4	1900±50	7x5x4
MDG_20	45.92	6.92641	1818	4.2	1900±50	14x13x7
MDG_33	45.92518	6.92299	1752	1-2	1100±50	14x11x4

Figure S 1: Images of englacial clast samples





MDG_18



MDG_18,19,



MDG_21,22



MDG_21,22,



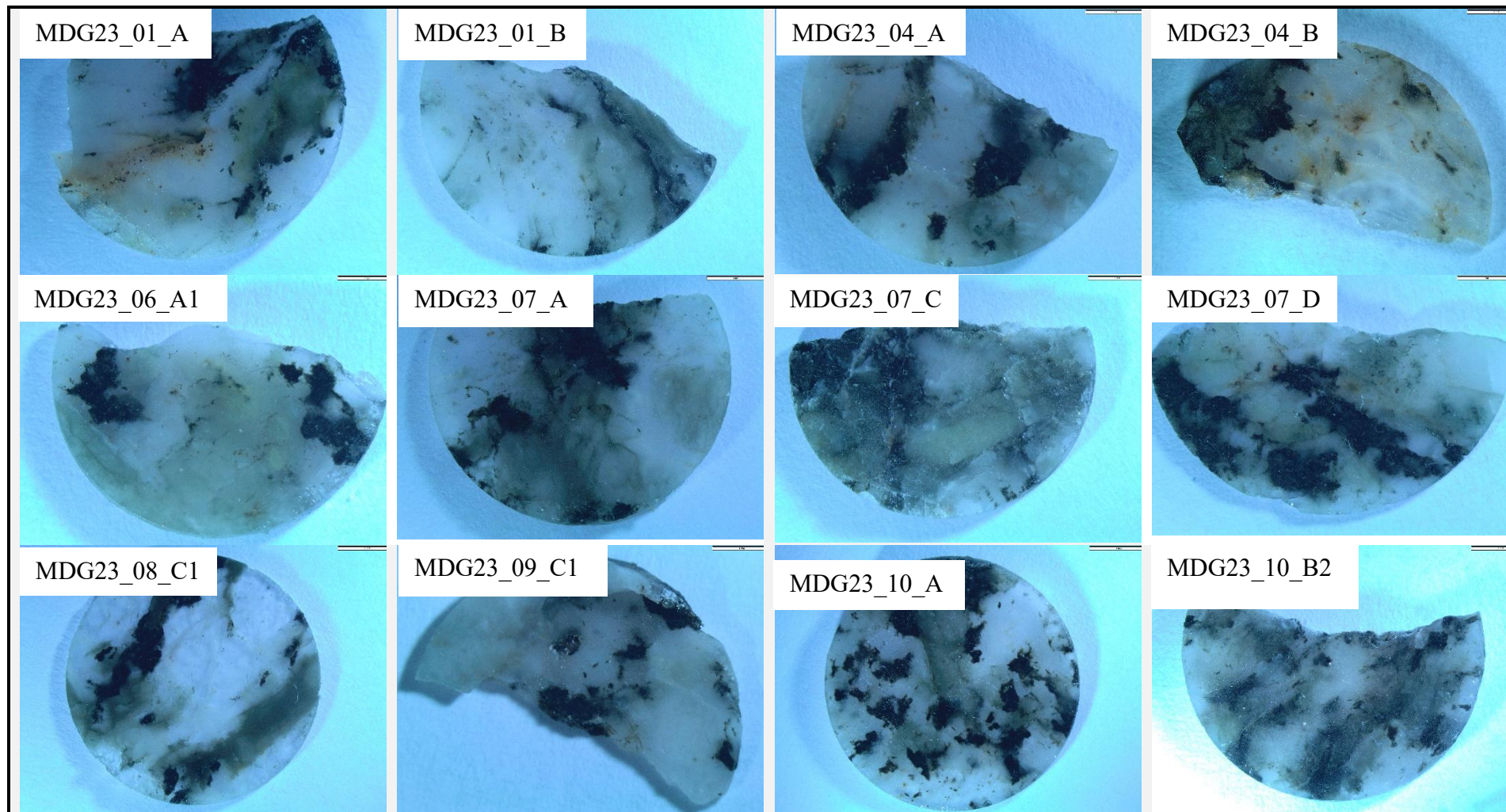
MDG_33

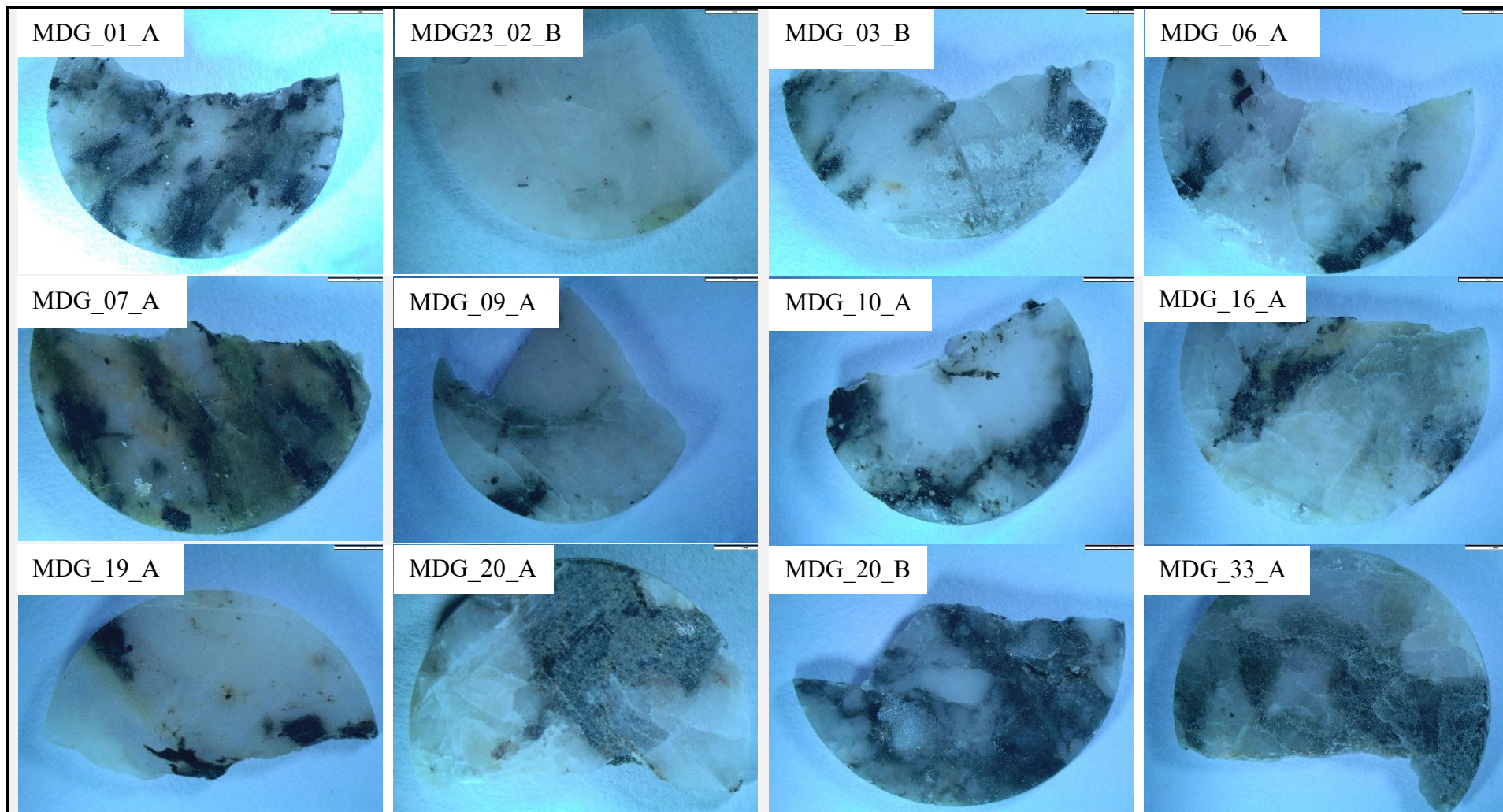


MDG_33



Figure S 2: Images of discs taken from cores of each of the englacial samples analysed. Each disc has a diameter of 16-18 mm.





2. Cosmogenic nuclide dating

TCN samples were prepared and measured at the Scottish Universities Environmental Research Centre AMS facility, East Kilbride, UK. The samples were crushed and sieved to separate the grains. The 250–500 μm fraction was washed, dried, and separated magnetically to recover the non-magnetic component. The samples were placed in a 6:1:1 solution of water, 37% HCl and 68% HNO₃ (aqua regia) on a hot plate (50°C) to remove organic matter, carbonates and soluble oxides. A mixture of 100:1 of water to concentrated (40%) HF was used to etch the feldspar and mica grains slightly, helped by placing the samples on a shaker table for one hour. The samples were then mixed with eucalyptus oil and placed into a surfactant solution to remove feldspar and mica grains by froth flotation (Herber, 1969). The floating minerals were discarded, and the remaining quartz grains recovered and placed into a solution of water, HF (40%), and HNO₃ at a ratio of 150:2:1 in a high-power ultrasonic tank for 24 hours, repeated three times to remove meteoric ¹⁰Be by isolating the quartz grain cores.

An aliquot of the quartz cores was sampled and tested for purity by dissolving and measuring the content of Al, Be, Fe, Ca, and Ti using ICP-OES. Samples that were not considered sufficiently pure were returned to the water, HF, and HNO₃ solution. Samples containing less than 175 ppm Al were dissolved in pure HF, and each sample was spiked with 0.2 mg of ⁹Be using an in-house carrier solution obtained from Phenakite. Once dissolved, the samples were dried to evaporate HF and converted to a chloride by the addition of HCl. The samples were then passed through an anion exchange chromatography column to remove Fe. The Fe-free samples were dried to evaporate all the HCl, and H₂SO₄ was added to convert the sample into a sulphate. The sample was then passed through a cation exchange chromatography column to remove the Ti and B, and to separate out the Al and Be fractions, eluted using HCl solutions. The remaining Be fractions were precipitated as hydroxides, and then oxidised at 900°C. The subsequent BeO was mixed with Nb at a ratio of 1:6 and pressed into copper cathodes for Accelerator Mass Spectrometer (AMS) analysis (Mendelová et al., 2020; Xu et al., 2010). ¹⁰Be concentrations ranged between 1.39×10^3 and 3.01×10^5 atoms per g. ¹⁰Be/⁹Be and were scaled to a nominal value of 2.79×10^{-11} ¹⁰Be/⁹Be or NIST SRM4325 standard (Nishiizumi et al., 2007). Procedural blank measurements ranged between 4% and 47% of the sample ¹⁰Be/⁹Be ratios.

3. Luminescence measurements

3.1 Sample preparation

All luminescence sample preparation and measurement were carried out at the University of Lausanne, Switzerland. Rock samples were cored into 16-18 mm diameter cores using a water-cooled rock drill and were sliced using a BUEHLER Isomet low speed saw and a lubricated (IsoCut) 0.3 mm thick diamond blade. Core lengths were 30-40 mm. For luminescence rock surface burial dating (RSBD) measurements, 15–20 slices per core were prepared with mean slice thickness of 0.76 ± 0.25 mm ($n = 665$).

3.2 Luminescence measurements

Luminescence measurements were made using a single Risø TL/OSL DA-20 reader equipped with a $\text{Sr}^{90}/\text{Yr}^{90}$ beta source and a DASH head following the protocol in Table S3. IRSL signals were detected in the blue part of the emission spectrum using a Schott BG39 and BG3 filter, whilst OSL measurements were detected in the UV part of the spectrum using a 7.5 mm Hoya U340 filter. Signals were integrated over the first 11.5 s of stimulation and the background signal over the final 50 s of stimulation. All measurements above 200 °C, were done under a nitrogen atmosphere. The instrument had a dose rate of $0.168\text{--}0.181 \pm 0.001$ Gy/s (average 0.175 Gy/s) over the measurement period. The instrument was calibrated using quartz slices gamma-irradiated with a known dose at the Institute of Radiation Physics of the University Hospital Lausanne (CHUV).

Luminescence profiles for all samples were plotted relative to sample depth. For luminescence RSBD samples, luminescence bleaching plateaus were evaluated following the approach of Freiesleben et al., (2015) to determine whether the sample had been fully bleached prior to burial. This comprises evaluating whether the measured luminescence signal in the rock surface burial dating sample is >5% different to what would be expected for an exposed sample and effectively comprises the limit of detection. Where this was the case, rock fragments from the plateaus were measured in a single aliquot regenerative dose (SAR) protocol (Table S3) to constrain the equivalent dose. Regenerative doses of 0, 1.75, 7, 14, 28, 56, 112 and 224 Gy were used and data were fitted using an exponential fit.

Table S 3: Single Aliquot Regenerative (SAR) protocol.

Treatment	Simulations details	Signal observed
1. Given dose, D_i	Natural/Regenerative Dose	
2. Preheat	251 °C, 60 s	
3. Light simulations	IRSL 50 °C, 230 s	IRSL ₅₀ L_n/L_i
	IRSL 225 °C, 230 s	IRSL ₂₂₅ L_n/L_i
	OSL 125 °C, 230 s	OSL ₁₂₅ L_n/L_i
4. Give test dose, D_t	250 s	
5. Heat	251 °C, 60 s	
6. Light simulations	IRSL 50 °C, 230 s	IRSL ₅₀ T_n/T_i
	IRSL 225 °C, 230 s	IRSL ₂₂₅ T_n/T_i
	OSL 125 °C, 230 s	OSL ₁₂₅ T_n/T_i
7. Hot bleach	290°C, 230 s	
8. Return to 1		

To confirm the quality of the measurements, residual doses were measured and a dose-recovery test conducted. Six new rock fragments in the saturated region (i.e. depth >12 mm from the surface) for each RSBD sample were exposed to artificial light for 24 hours in a solar simulator (uvaCUBE 400). Three fragments were then

given a dose of ~ 19 Gy, which corresponds to the largest D_e recorded for the IRSL₂₂₅ signal of core MDG23_04_A1, whilst the remaining three fragments were not dosed prior to measurement.

Anomalous fading was measured for each sample following Auclair et al., (2003). Two previously measured fragments were dosed before preheating, and were measured following different delay times ranging from 0 to 3000 s. Fading rates were calculated using Analyst v. 1.23, and ages were fading corrected following Huntley & Lamothe, (2001) using the function `calc_FadingCorr` (Kreutzer et al., 2017) in the R Luminescence package. For $g_{2\text{days}}$ -values < 1 %/decade, no fading correction was made (Buylaert et al., 2009).

3.3 Environmental dose rate determination

Environmental dose rates were calculated following either high-resolution Ge detector gamma-ray spectrometry at the University of Lausanne or ICPMS measurements made at Actlabs, Canada, dependent on sample size. Calculations were only done for RSBD samples that passed the plateau test described above. Sample grain sizes were estimated based on optical microscopy (Fig. S2) and range from 100 to 2000 μm . Most of the samples exhibit grain size variability, with implications for the calculated beta dose rate, introducing age uncertainties of hundreds of years. This limitation affects all luminescence studies on bedrock, and we opt to use the average grain size of 850-950 μm for our age calculations. As our samples are embedded in ice, we assumed that only the external dose component is related to the cosmic dose rate. We estimated ice thickness at 100 m; increasing the ice thickness to 200 m exhibits no impact on the calculated cosmic dose rate. Furthermore, the clasts that we analysed are not perfectly spherical, which may impact our gamma scaling calculation (e.g. Riedesel & Autzen, (2020)). We opted to use the average axis length to estimate our clast diameters but also explored the effect of using the clast long-axis length on the f_a scaling calculation. For example, for sample MDG23-01 this increased the clast diameter from 11 cm to 16 cm and resulted in a 3% change in the total dose rate and resultant age. Uncertainty in clast diameter thus causes a difference in age of a few decades, which is negligible. Environmental dose rates at the rock surface vary between 0.8 ± 1.3 Gy ka^{-1} and 7.33 ± 0.4 Gy ka^{-1} (Table 2 & S7).

3.4 Luminescence rock surface exposure dating results

Luminescence bleaching profiles were measured from two cores of each of the four calibration samples. We used a general order kinetic model of luminescence signal bleaching in rock surfaces (GOK, Biswas et al., 2023; Freiesleben et al., 2023; Pathan et al., 2024) to fit each of our calibration samples to obtain the kinetic parameters that describe luminescence signal loss. Note that it was only possible for one core of samples MDG-HF-03 and MDG-HF-04 to be fitted because the measured data did not reach a saturation plateau in the other cores (cores too short). An approach after (Lehmann et al., 2019) was used to confirm that the obtained kinetic parameters were robust, whereby different calibration samples were used to predict the luminescence exposure age of a further sample excluded from the calibration (Table S25, S26, S27). Some variability in predicted ages was obtained, however all three signals yield ages that are within uncertainty of the known age

of 1 year: IRSL_{50} : 1.60 ± 0.50 , IRSL_{225} : 0.87 ± 0.13 and OSL_{125} : 0.94 ± 0.29 . All samples were thus used to obtain the kinetic parameters (Figure S3) that are given in Table S4.

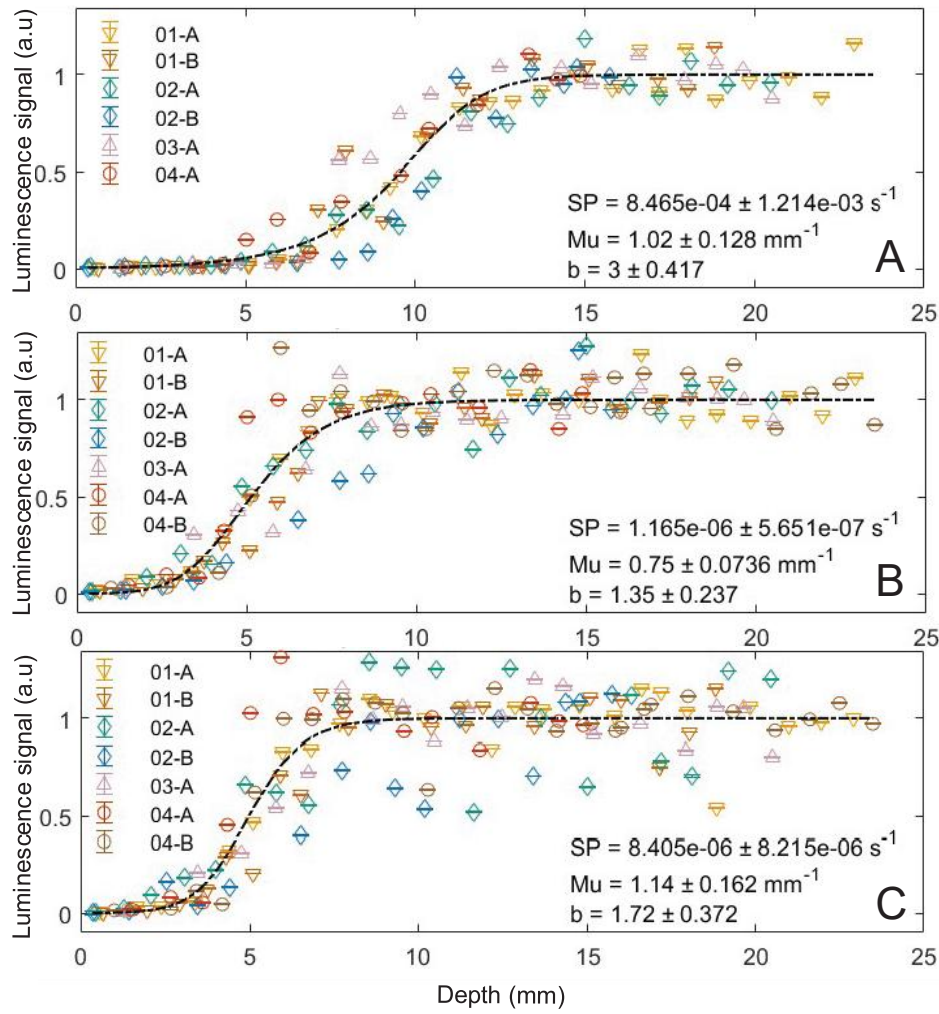


Figure S 3: Calibration depth profiles and fitting parameters for the different signals
A) IRSL_{50} , B) IRSL_{225} , C) OSL_{125} . Colours indicate different cores and shapes different samples. Cores 03B and 04B (IRSL_{50} only) do not extend to the saturated part of the profile and have been excluded.

Table S 4: Luminescence bleaching parameters for the headwall samples

Signal	$\sigma\phi_0$	μ	b
IRSL_{50}	$8.464 \times 10^{-4} \pm 1.214 \times 10^{-3}$	1.023 ± 0.128	3.000 ± 0.417
IRSL_{225}	$1.165 \times 10^{-6} \pm 5.651 \times 10^{-7}$	0.750 ± 0.074	1.348 ± 0.237
OSL_{125}	$8.405 \times 10^{-6} \pm 8.215 \times 10^{-6}$	1.144 ± 0.162	1.724 ± 0.372

Using the parameters listed in Table S4, it was possible to fit the unknown luminescence exposure profiles to obtain ages that ignore the potential effect of erosion. Ages are consistent within the same core for the different signals, generally yielding exposure ages that range between ~ 1 year and ~ 100 years, except for one core of sample MDG-HF-04 and MDG-HF-01 that give older ages (Table S5).

Table S 5: Luminescence RSED results

Sample	Core	IRSL ₅₀ (year)	IRSL ₂₂₅ (year)	OSL ₁₂₅ (year)
MDG-HF-01	1	1.66 ± 0.13	1.60 ± 0.10	1.60 ± 0.13
MDG-HF-01	2	191.10 ± 26.76	13.96 ± 1.30	64.65 ± 11.57
MDG-HF-01	1&2	14.17 ± 2.32	4.17 ± 0.36	8.29 ± 1.23
MDG-HF-02	1	60.61 ± 3.53	11.06 ± 0.51	33.61 ± 3.50
MDG-HF-03	1	5.11 ± 0.80	16.02 ± 2.04	93.18 ± 24.40
MDG-HF-03	2	0.65 ± 0.12	2.44 ± 0.13	6.28 ± 0.64
MDG-HF-03	1&2	2.15 ± 0.28	5.23 ± 0.51	21.31 ± 3.91
MDG-HF-04	1	5.45 ± 0.80	12.05 ± 1.17	64.05 ± 4.38
MDG-HF-04	2	481.19 ± 34.21	21.08 ± 2.26	111.35 ± 8.04
MDG-HF-04	1&2	91.63 ± 19.04	14.87 ± 1.07	78.66 ± 4.08

3.4.1 Inverting for erosion rates

A paired erosion rate inversion was done for the luminescence and cosmogenic nuclide data, using the approach of Lehmann et al., (2019a; 2019b), modified to use the general-order kinetic model to fit the luminescence data (Freiesleben et al., 2023; Pathan et al., 2024). The inversion assumes that erosion rates evolve through time with increasing erosion towards the present-day. Initially a reference profile for the luminescence signal is calculated, based on the ^{10}Be age assuming zero erosion (t_0). The inversion then solves for a corrected (older) exposure age (t_c) that satisfies both the luminescence and ^{10}Be data. Erosion histories are inferred for different erosion rates, $\dot{\epsilon}$, and pairs of t_c and t_s , where t_s is the onset time of erosion. We explored $\dot{\epsilon}$ of between 10^{-2} to 10^{-6} m a^{-1} and t_s of 0.1 to 1000 years. Inversion results are shown in Figs S4 – S15. For the IRSL₅₀ and OSL₁₂₅ signals, two cores yield erosion rates that are outside of the model bounds, ie. $<10^{-6} \text{ m a}^{-1}$ at steady state. We consider erosion rates $<10^{-6} \text{ m a}^{-1}$ to be beyond the resolution of the luminescence RSED technique.

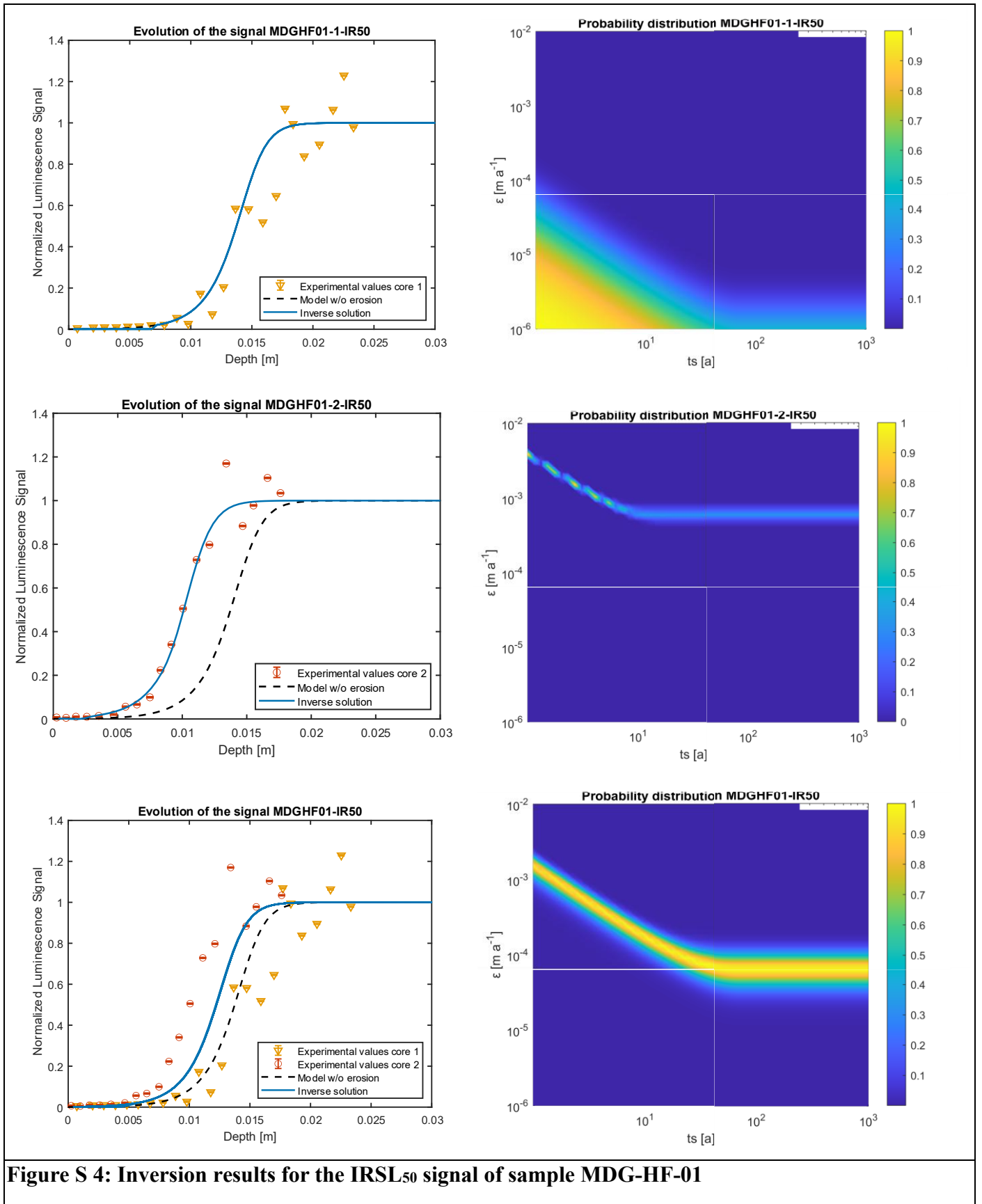


Figure S 4: Inversion results for the IRSL₅₀ signal of sample MDG-HF-01

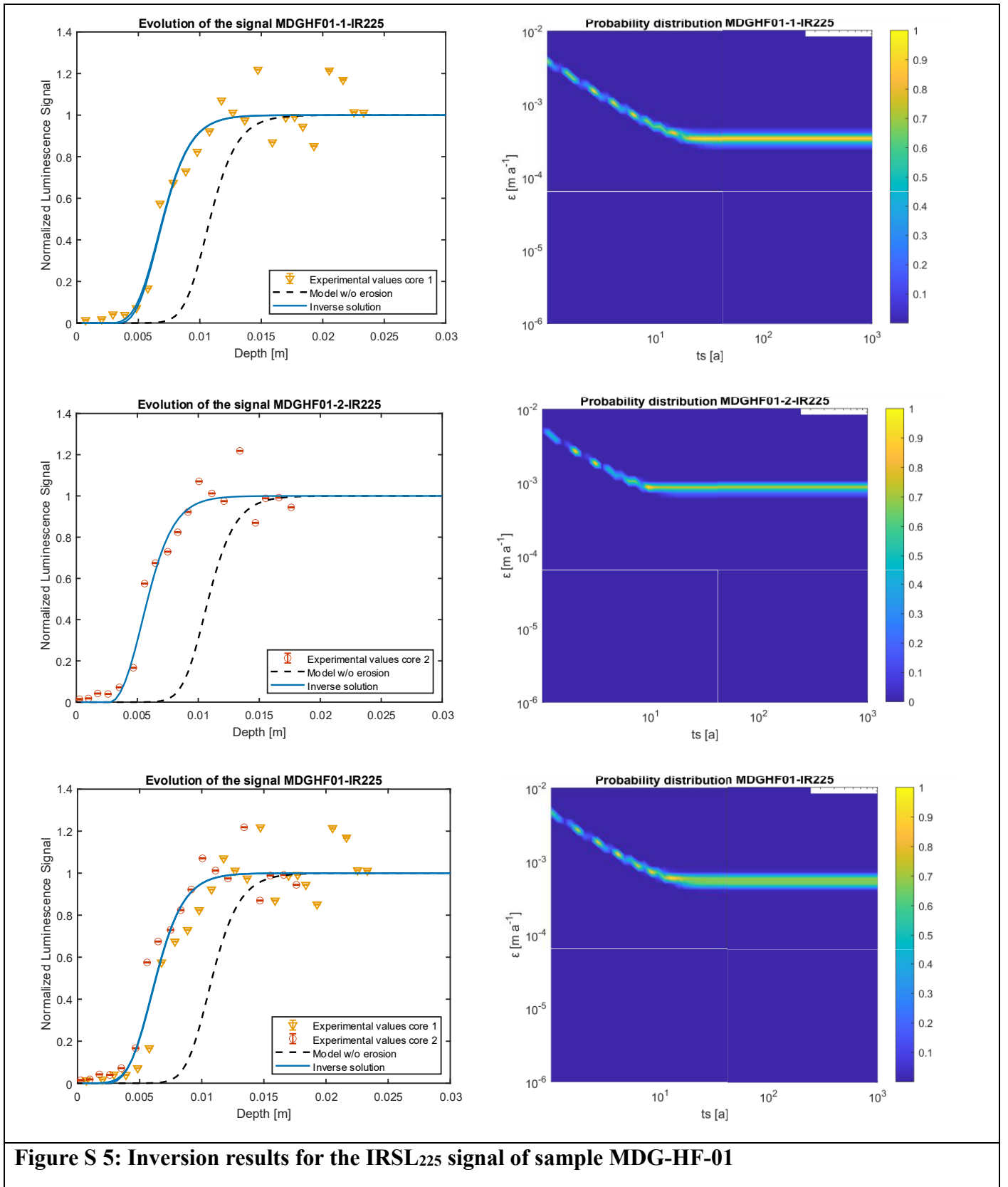


Figure S 5: Inversion results for the IRSL₂₂₅ signal of sample MDG-HF-01

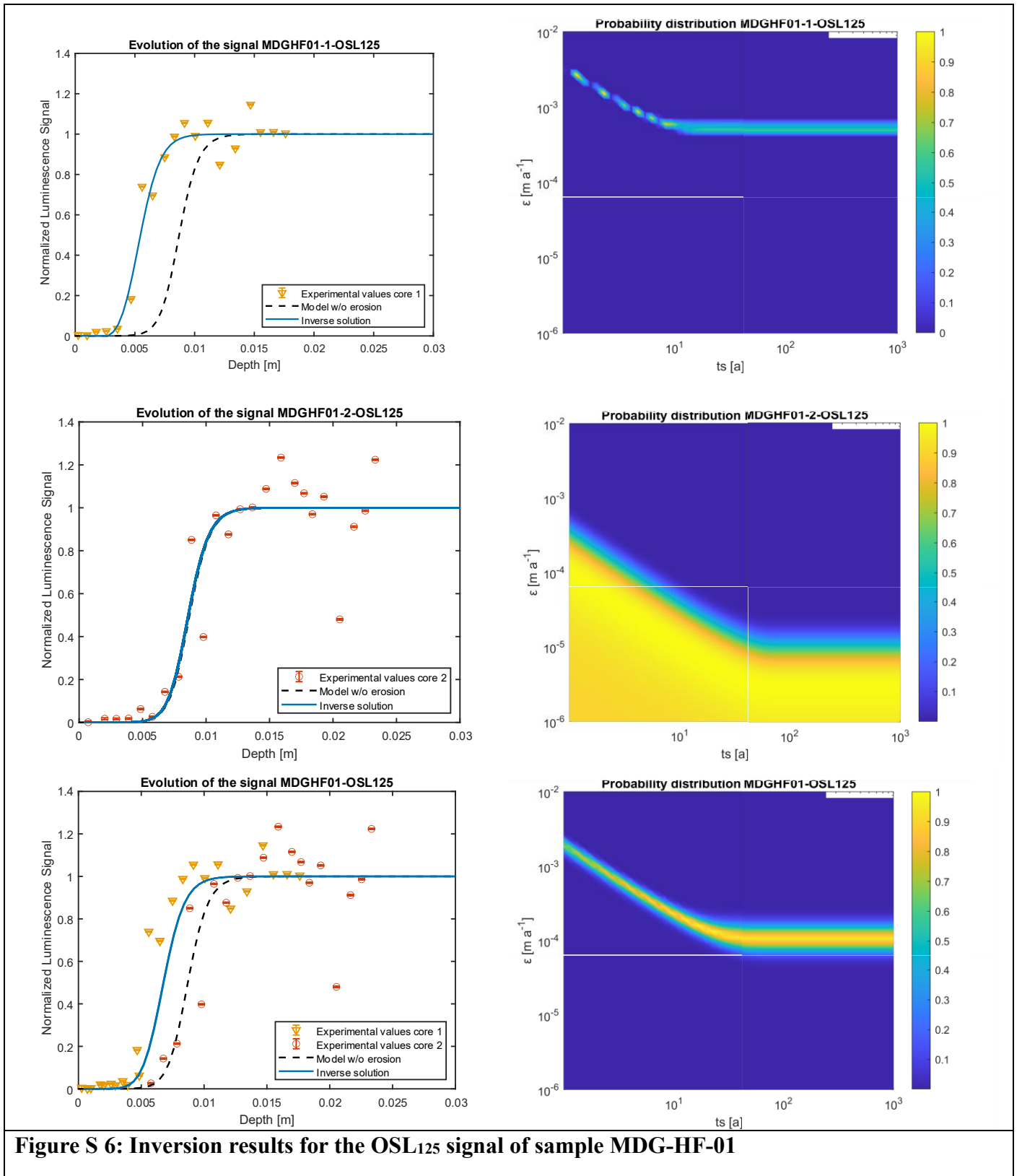


Figure S 6: Inversion results for the OSL₁₂₅ signal of sample MDG-HF-01

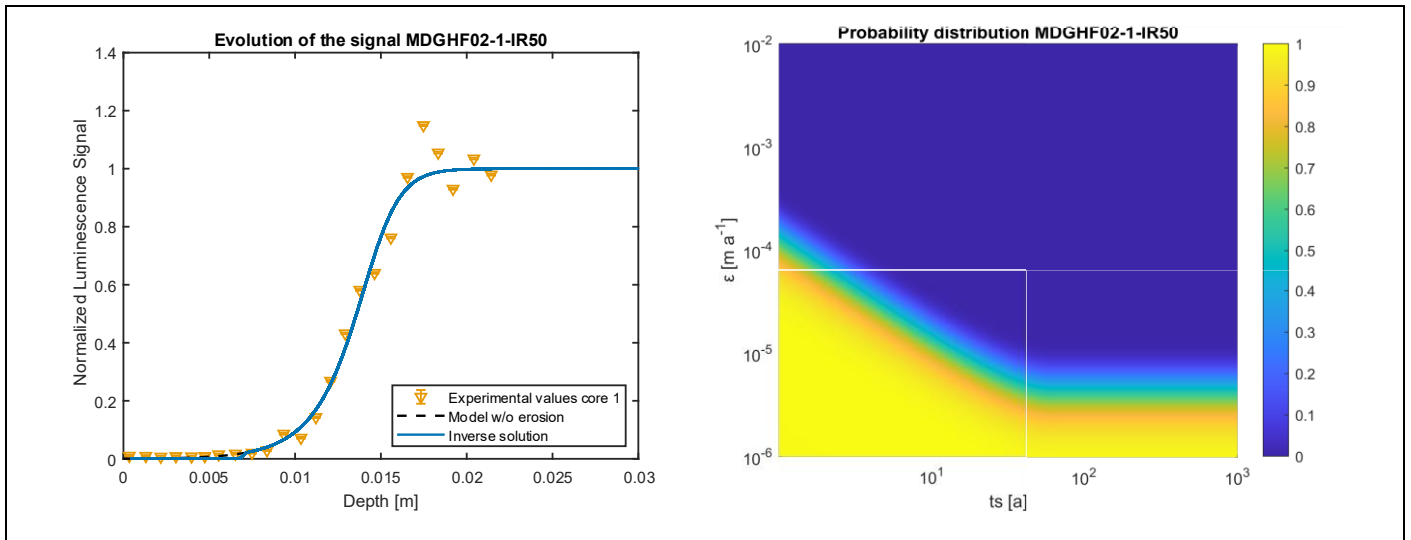


Figure S 7: Inversion results for the IRSL₅₀ signal of sample MDG-HF-02

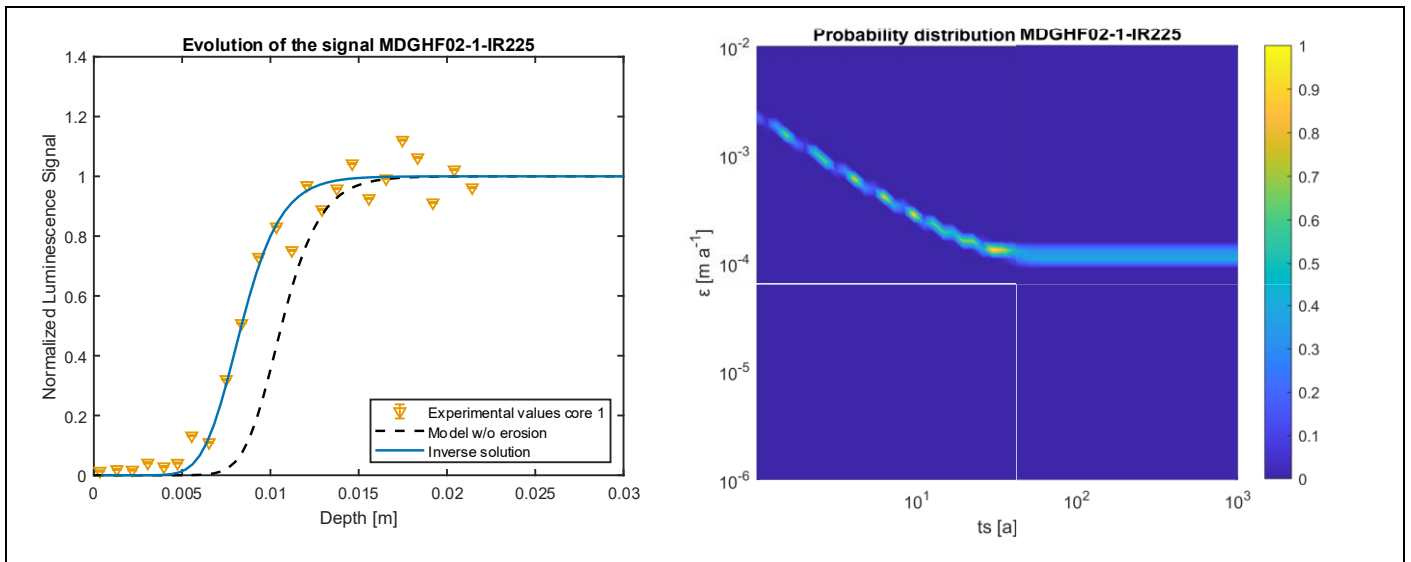


Figure S 8: Inversion results for the IRSL₂₂₅ signal of sample MDG-HF-02

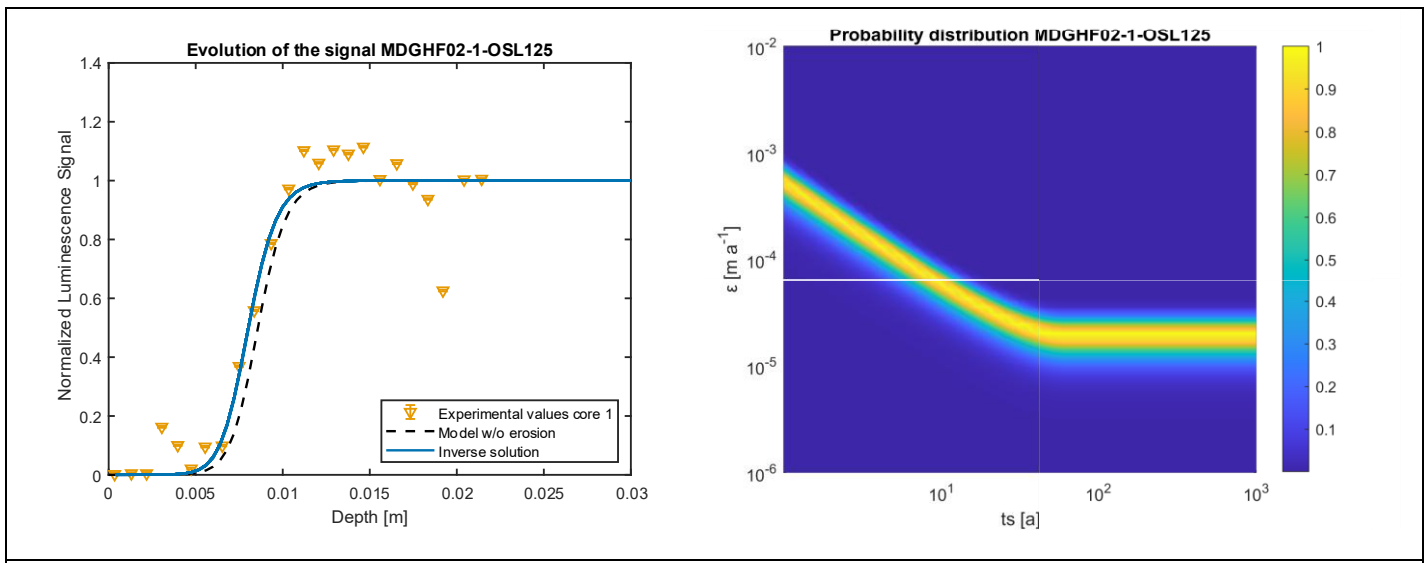


Figure S 9: Inversion results for the OSL₁₂₅ signal of sample MDG-HF-02

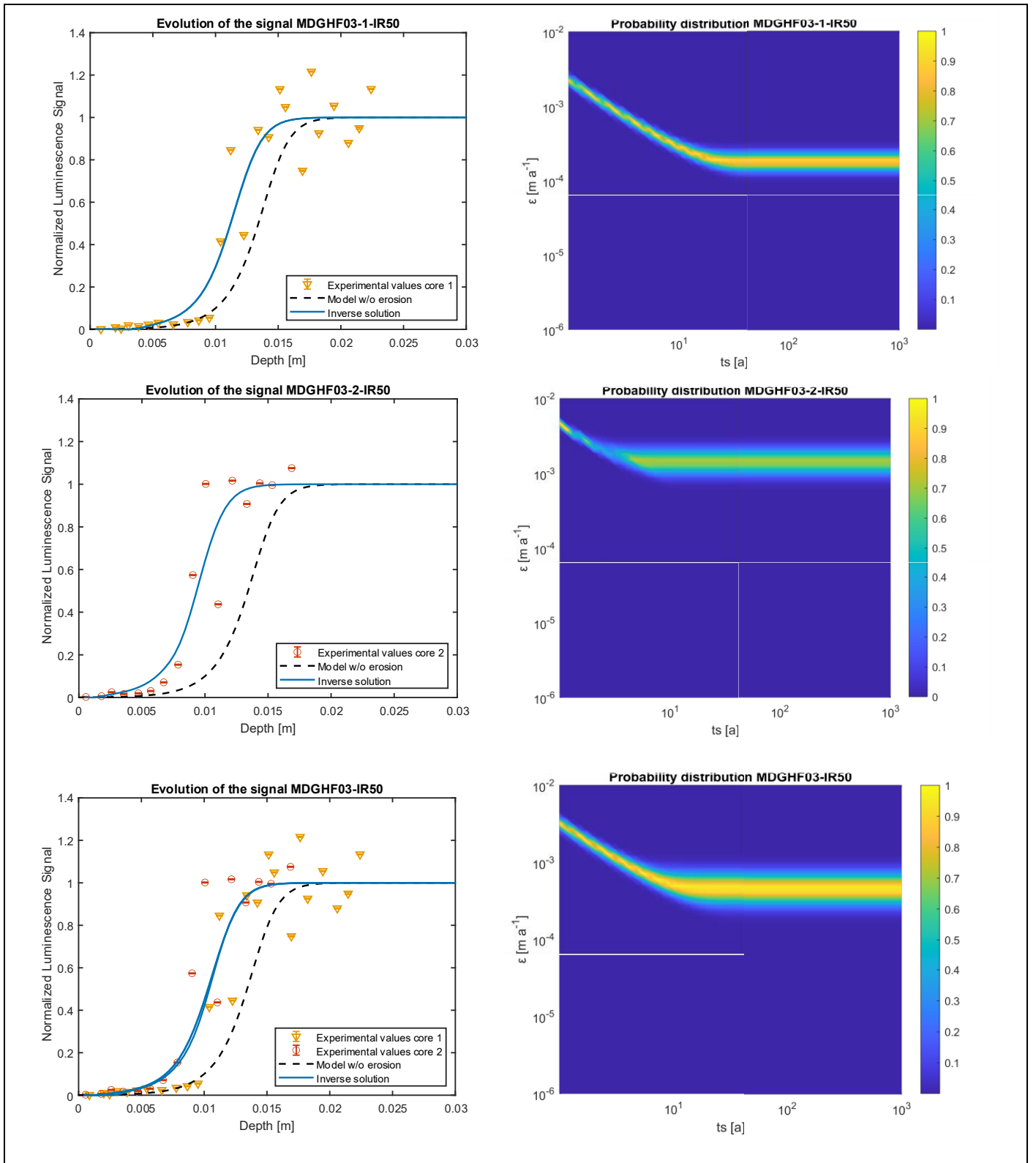


Figure S 10: Inversion results for the IRSL₅₀ signal of sample MDG-HF-03

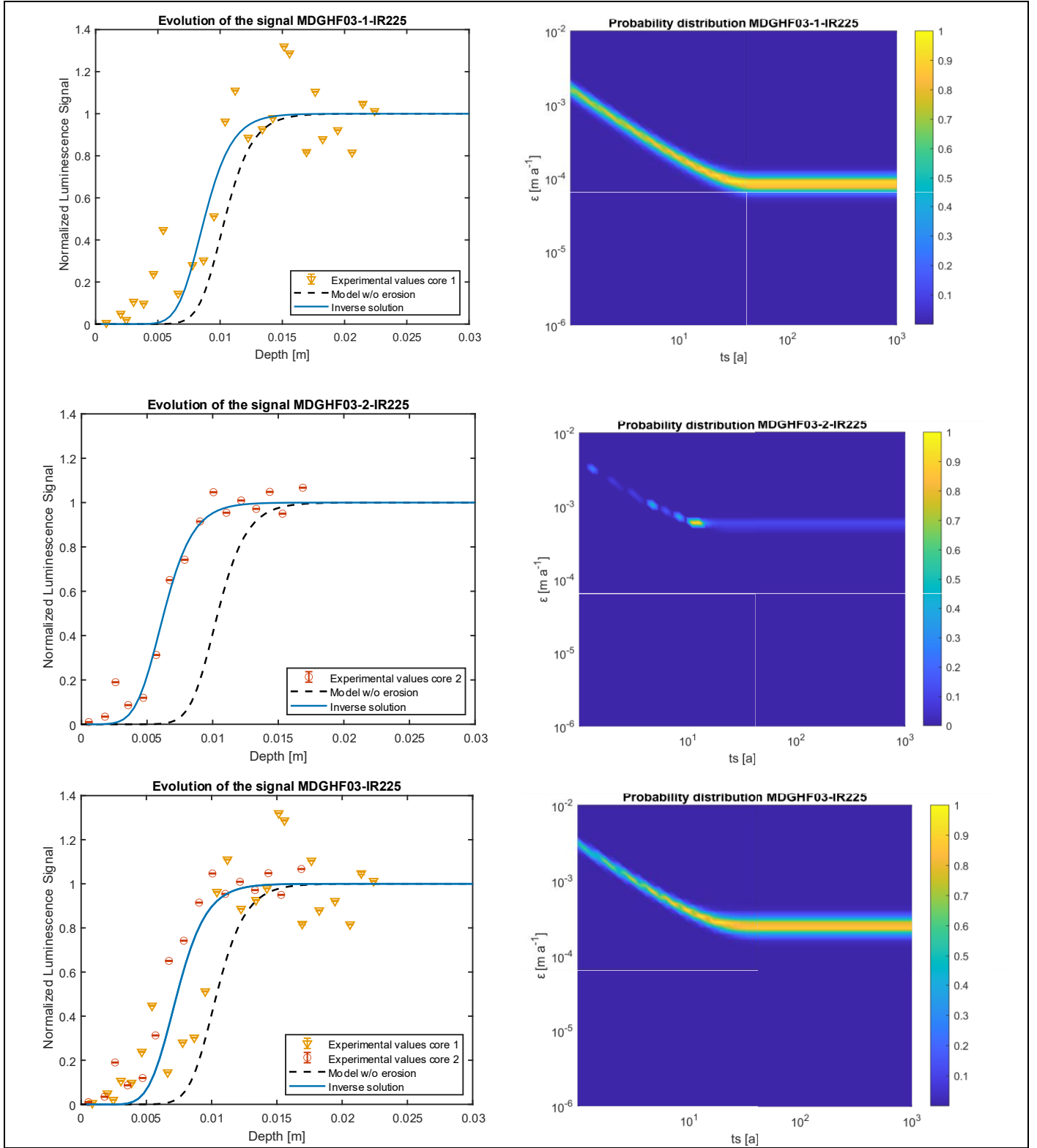


Figure S 11: Inversion results for the IRSI₂₂₅ signal of sample MDG-HF-03

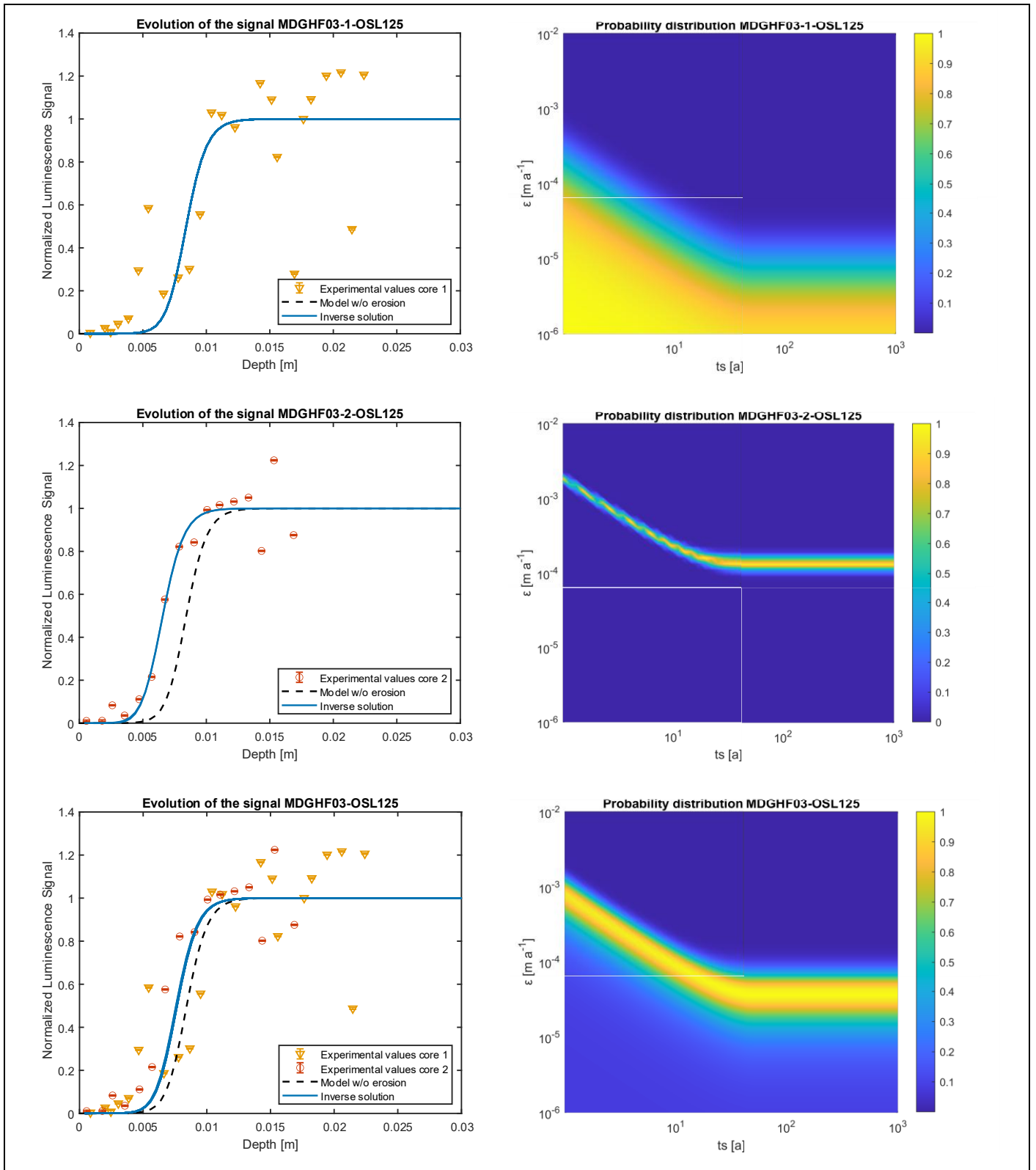


Figure S 12: Inversion results for the OSL₁₂₅ signal of sample MDG-HF-03

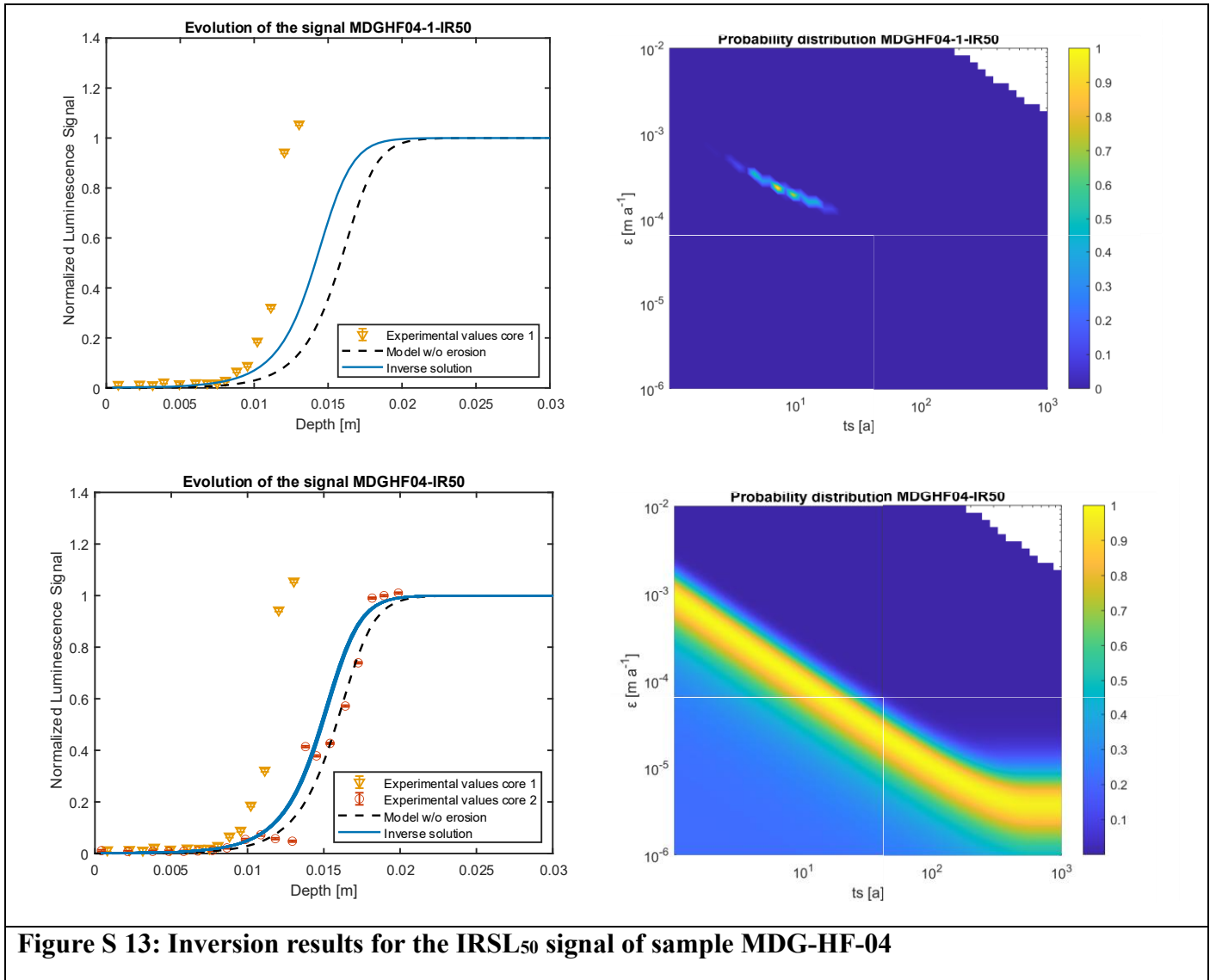
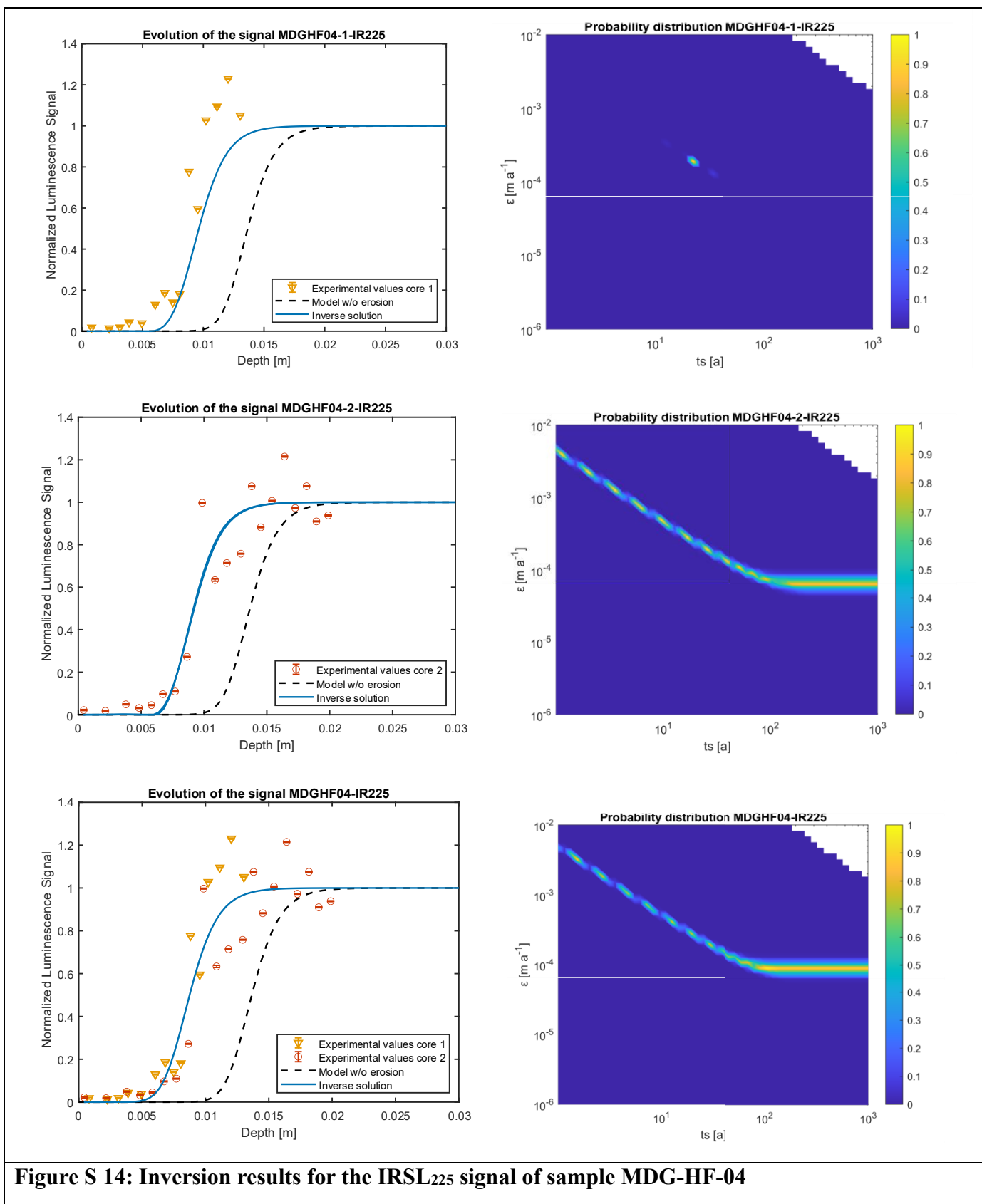
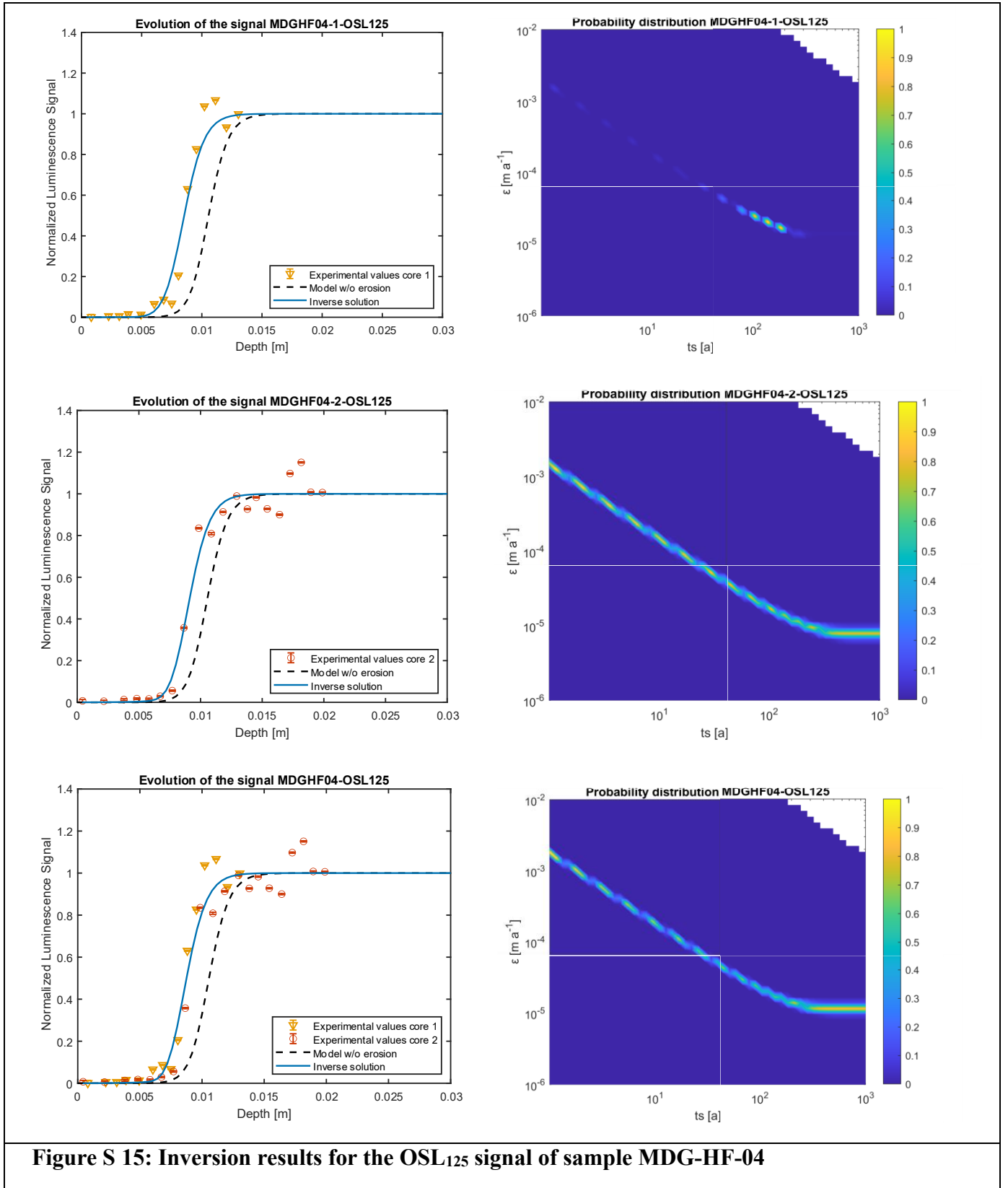


Figure S 13: Inversion results for the IRSL₅₀ signal of sample MDG-HF-04





3.5 Luminescence rock surface burial dating results

38 cores were taken from the 27 samples collected from the Mer de Glace. For the IRSL₅₀ signal, 19 samples (24/38 cores) yield an L_n/T_n bleaching plateau with 2-9 rock fragments passing the plateau test, for the IRSL₂₂₅ signal 11 samples (14/38 cores) yield a bleaching plateau with 2-10 rock fragments, and for the OSL₁₂₅ signal, 8 samples (11 cores) yield a bleaching plateau with 2-5 rock fragments (Figs S17 – S25). Bleaching plateaus for IRSL₂₂₅ signals are generally shorter than those of the IRSL₅₀ signal, which is likely related to the slower bleaching rate of IRSL₂₂₅ signals (e.g. Colarossi et al., 2015).

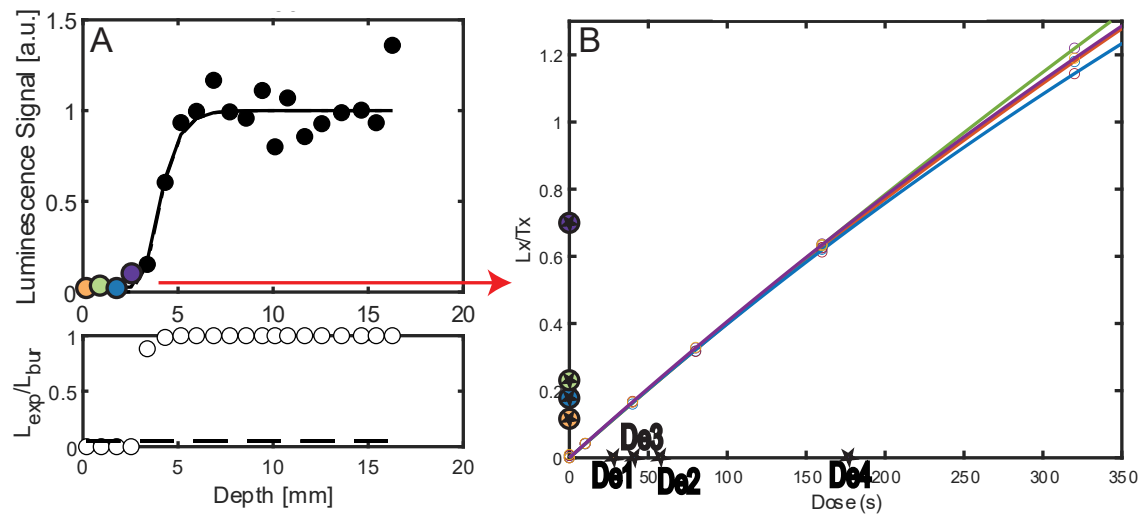


Figure S 16: Luminescence bleaching profile for the IRSL₅₀ signal of sample MDG23 (core 10-B2) (A) and the corresponding SAR dose response curves (B) measured for fragments on the bleaching plateau (see colours).

Except for sample MDG_32, all dose-response curves (Figs S26-S40) fulfilled the acceptance criteria of a recycling ratio <10 %, $L_n > 3\sigma$ above background and recuperation <5 %. Dose-response curves were fitted using a single saturating exponential fit until the maximum given dose of ~56 Gy (320 s), which encompasses the natural signal of each sample and signal.

Fading rates vary with g_{2days} -values ranging from 2.93 ± 0.23 % decade⁻¹ to 9.03 ± 0.13 % decade⁻¹ for the IRSL₅₀ signal and from 0.65 ± 0.92 % decade⁻¹ to 3.6 ± 0.31 % decade⁻¹ for the IRSL₂₂₅ signal (Table S7, S8, Fig. S41). Ages were fading corrected except for MDG23_01 IRSL₂₂₅ where the fading rate is within 1%/decade (Buylaert et al., 2009b). Fifteen samples yield ages. Of these, 13 yield ages younger than 2.5 ka. Within this subset, five samples are <1 ka, five 1-2 ka, and three 2-2.5 ka and there is a slight trend towards younger ages for cores with long plateaus (Fig. S44).

The D_e values derived from IRSL₂₂₅ signals are often greater than IRSL₅₀ signals, and the bleaching plateaus are shorter. This difference could be explained by slower bleaching of IRSL₂₂₅ signals (Colarossi et al., 2015). No OSL₁₂₅ measurements passed the dose-recovery test within 10% of unity, the cause of this is unclear. Thus, given the increased bleaching of IRSL₅₀ signals, we opted to use these signals only for the determination of surface burial ages of englacial clasts. Residual doses ranged from 0.24 ± 0.12 to 3.31 ± 7.54

and have not been subtracted from the ages. Three reasons support this choice: 1) the dose-recovery ratio is more accurate where residuals are not subtracted for most of the samples; 2) the natural luminescence signal is completely bleached at the rock surface in L_n/T_n bleaching profile from bedrock in Trélaporte (granite, Mer de Glace) (Lehmann, et al., 2019b), suggesting that the residual values for the Mont-Blanc granite are overestimated, 3) the fragments measured for the residual dose may not be representative of the residual dose of those measured for equivalent dose determination.

Rock fragment ages from the plateau of a single core are variable for some samples fulfilling the plateau test (Freiesleben et al., 2015) (Fig. S43). This variability may be related to mineralogical heterogeneity between the rock fragments analysed, which influences the luminescence measurements, the fading rate and the environmental dose rate. Rock fragments that yield fading-corrected ages $>1\sigma$ different to the average of all rock fragment fading-corrected ages on the plateau are considered to be outliers and have been excluded from the calculation of the average age (Table S7). For samples with a long plateau, the results vary little even following exclusion of outliers, however for samples with shorter plateaus the ages may become younger by a few decades to a few hundred years.

Figure S 17: Luminescence bleaching profiles of RSBD samples: MDG23-01 (A2,B1), 02 (A2), 03 (A1).

Accepted cores have coloured aliquots on the bleaching plateau. Rock fragment signals that yield ages that are $>1\sigma$ different to the average of all rock fragment ages that pass the plateau test are coloured yellow and those retained for the “final” ages are coloured red. Grey indicates rock fragments that pass the plateau test but do not fulfill the signal acceptance criteria (e.g. error in DRC or DRR $>10\%$) (Table S73).

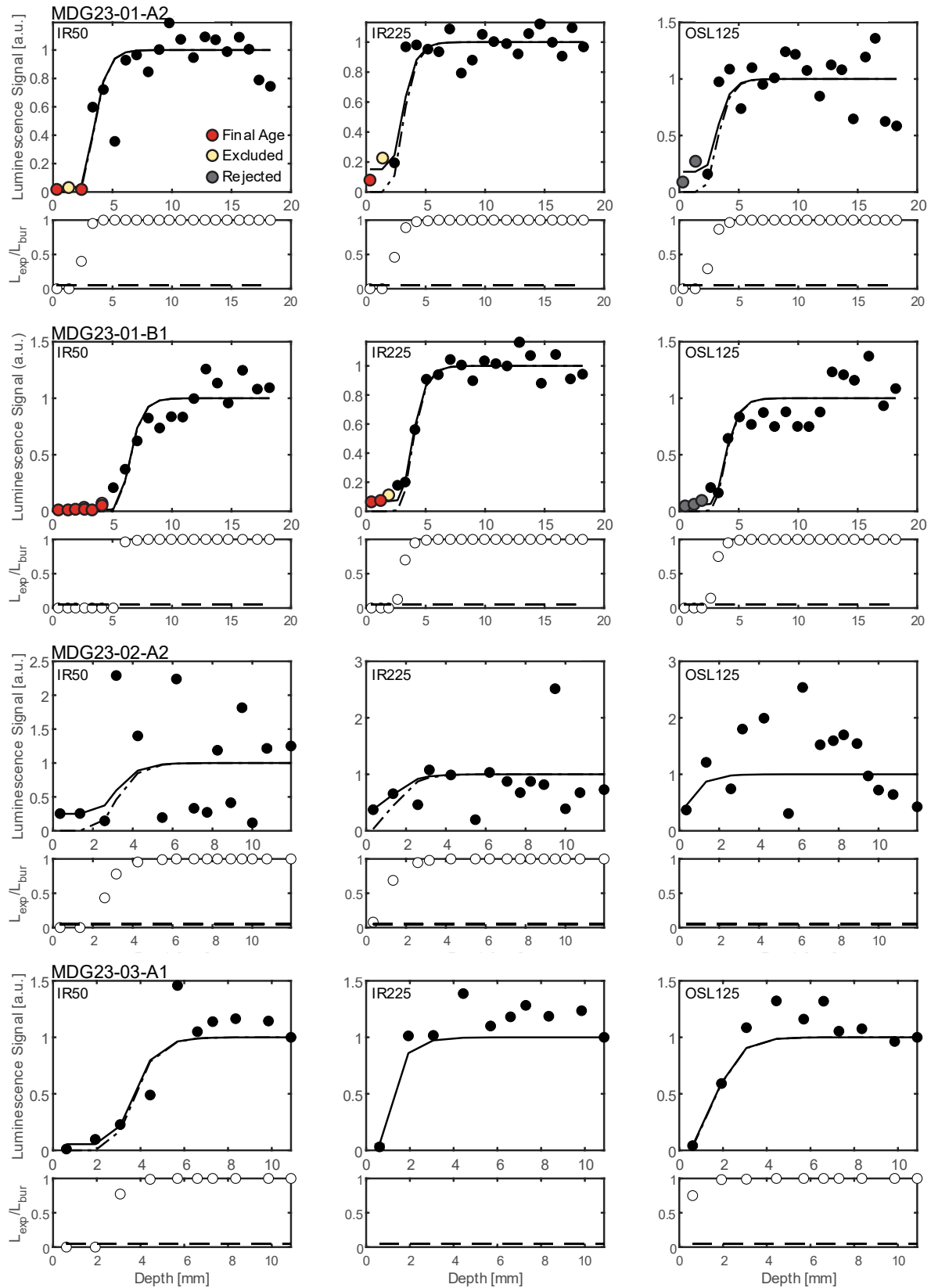


Figure S 18: Luminescence bleaching profiles of RSBD samples: MDG23-03 (A2), 04 (A1,B1), 05 (A1).

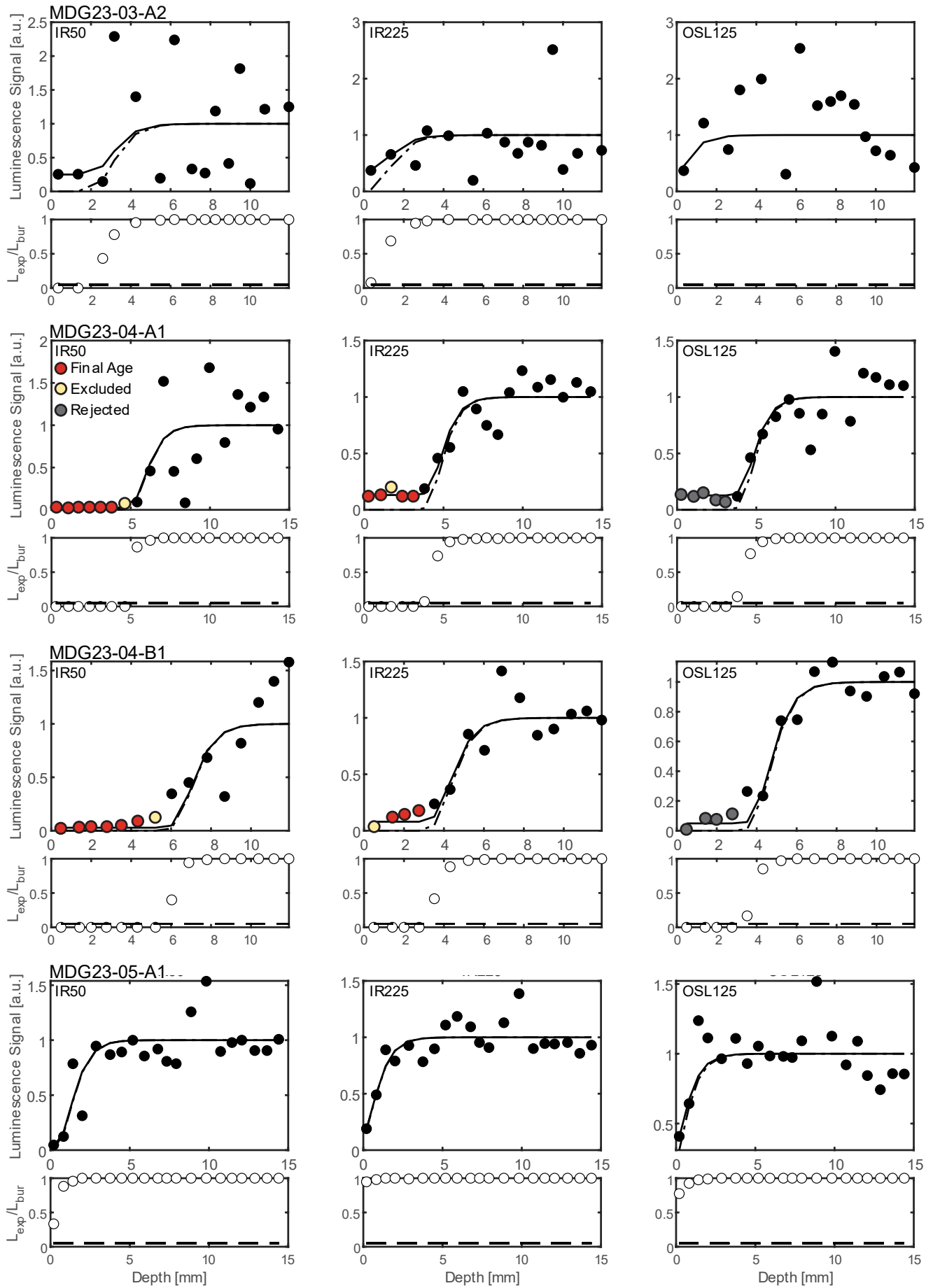


Figure S 19: Luminescence bleaching profiles of RSD samples: MDG23-06 (A1), 07 (A1,B1,C1).

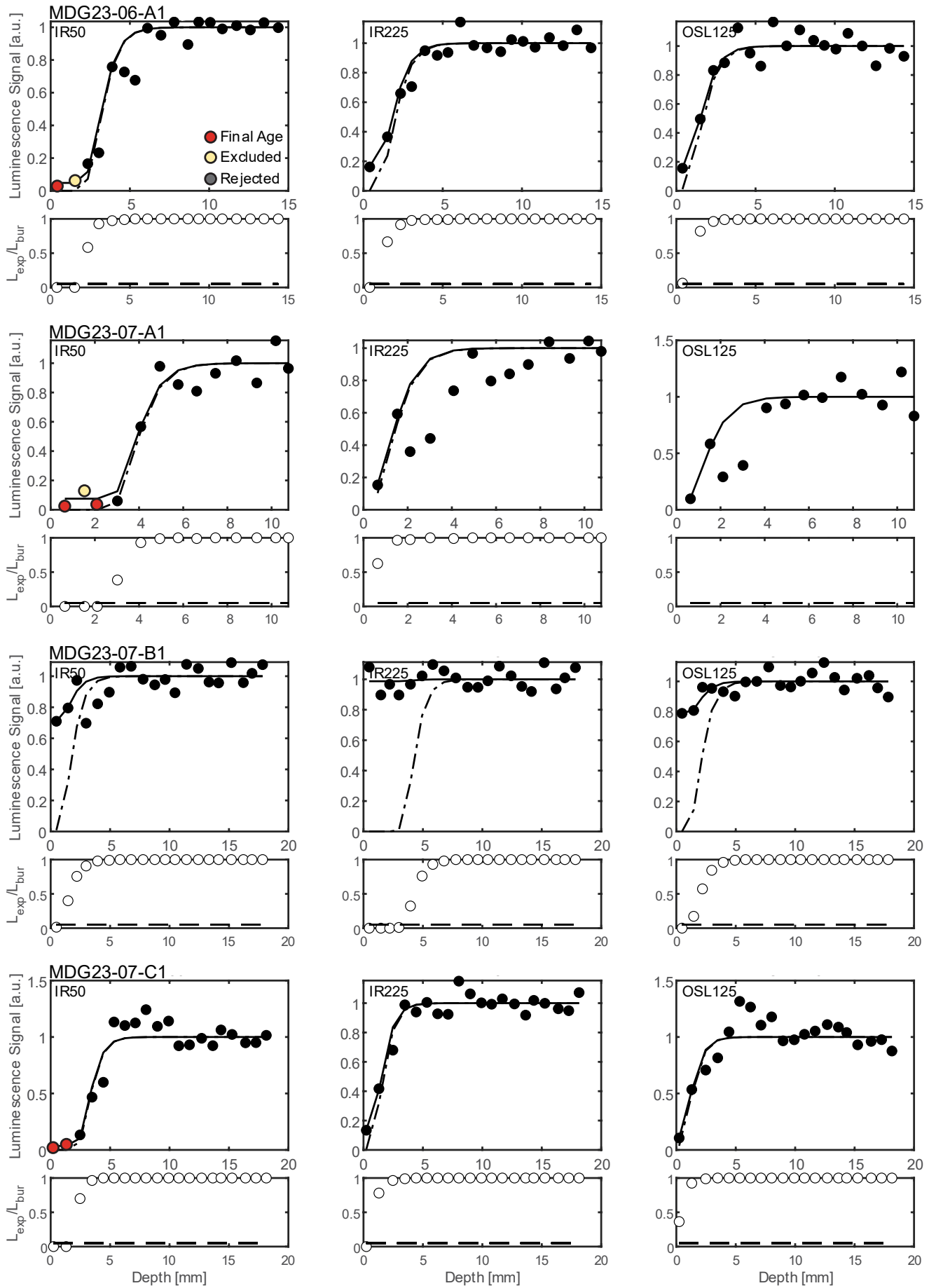


Figure S 20. Luminescence bleaching profiles of RSBD samples: MDG23-07 (D1), 08 (A1,C1), 09 (A1).

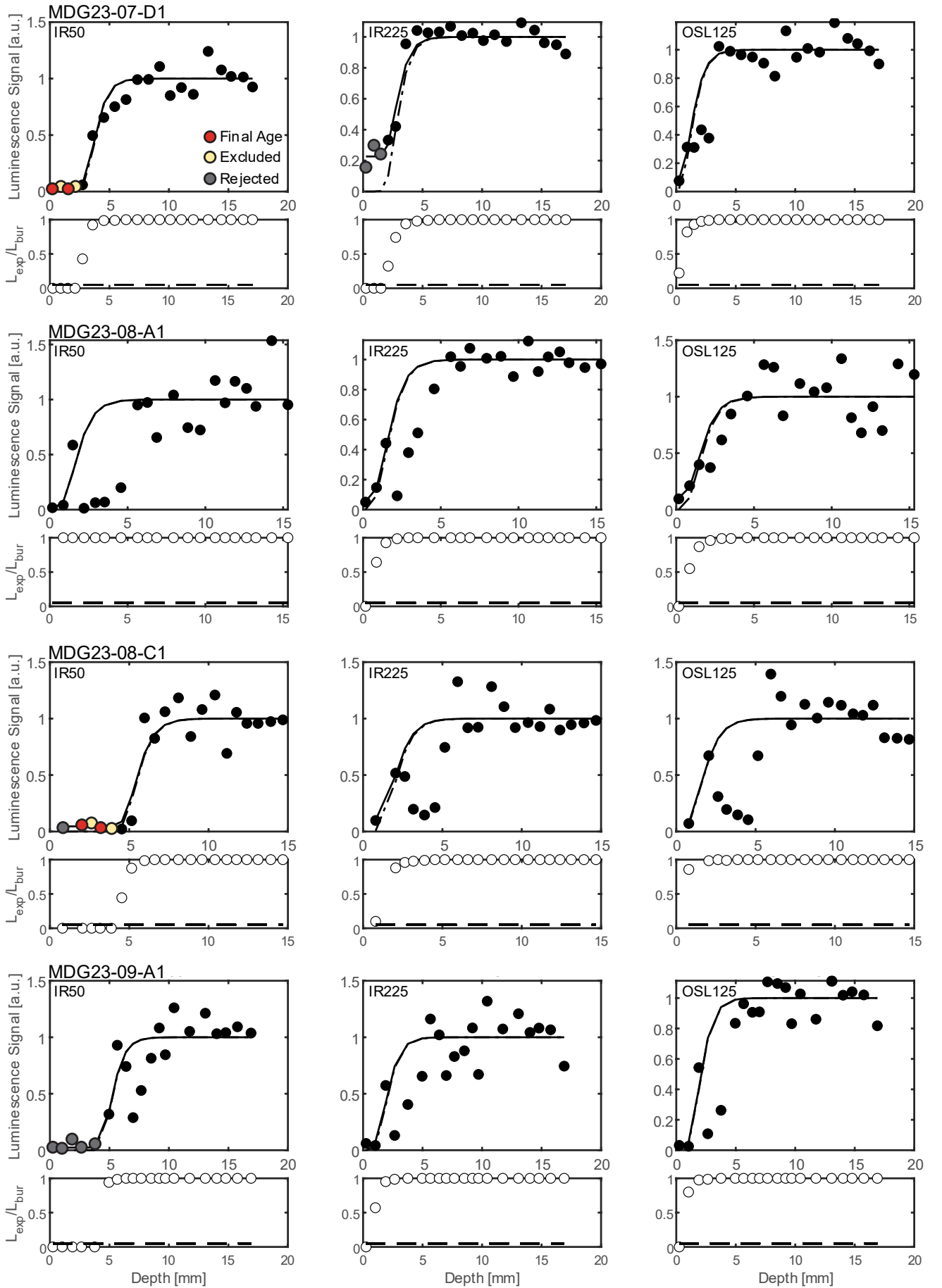


Figure S 21: Luminescence bleaching profiles of RSBD samples: MDG23-10 (A2,B2), MDG-01 (A), 02 (A).

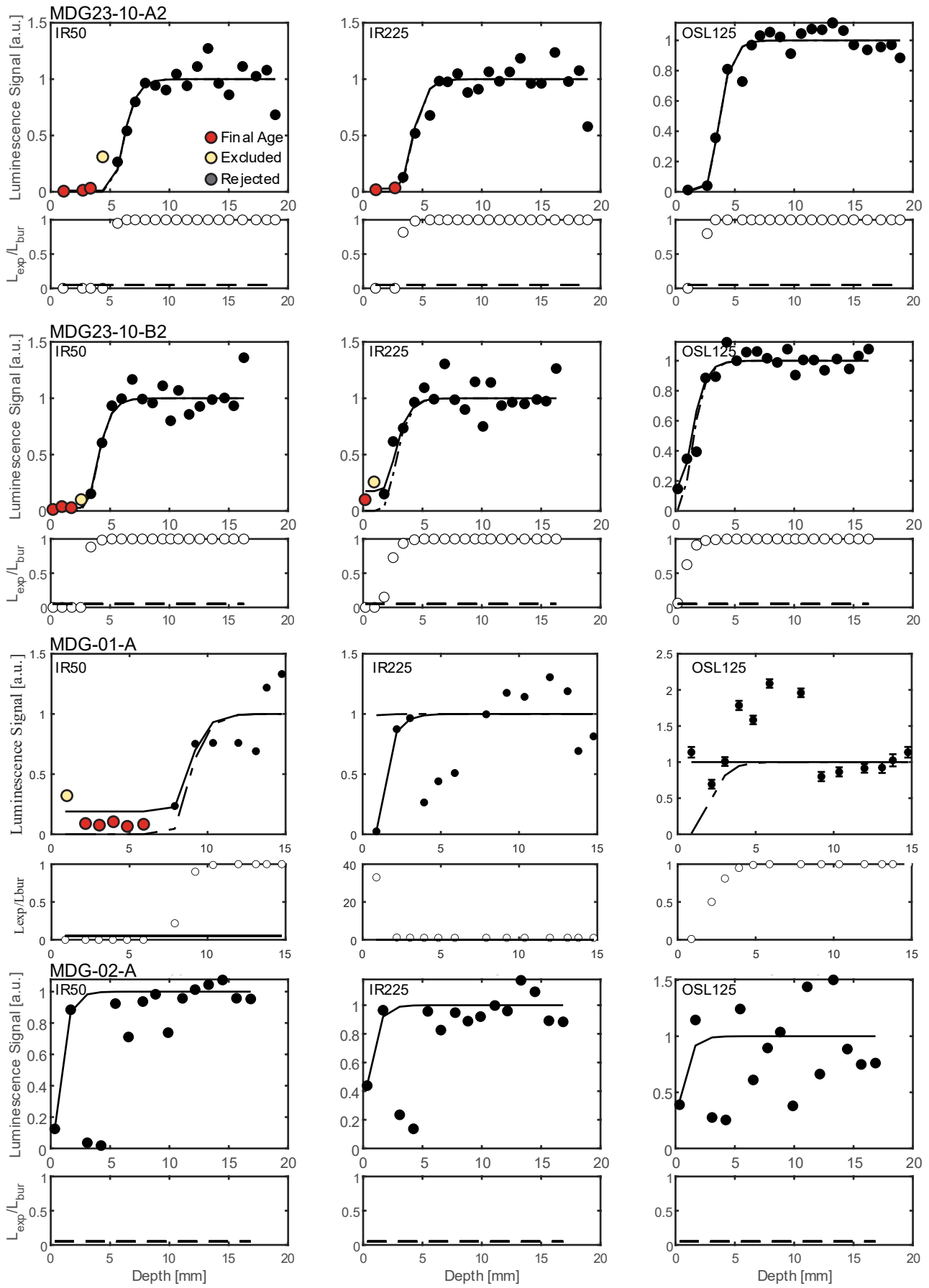


Figure S 22: Luminescence bleaching profiles of RSBD samples: MDG-02 (B1), 03 (B), 06 (A), 07 (A).

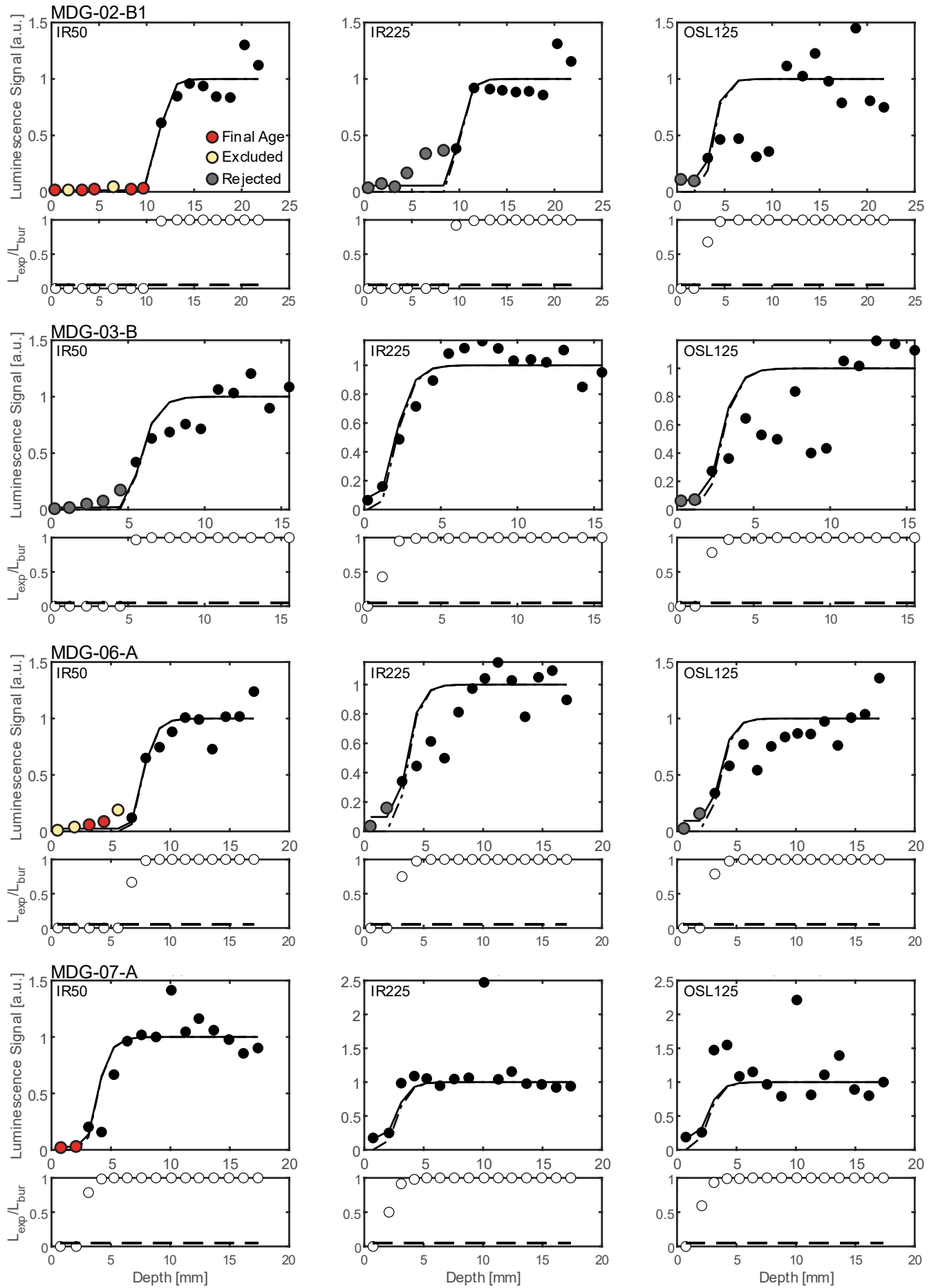


Figure S 23: Luminescence bleaching profiles of RSBD samples: MDG-09 (A), 10 (A), 13 (A), 16(A).

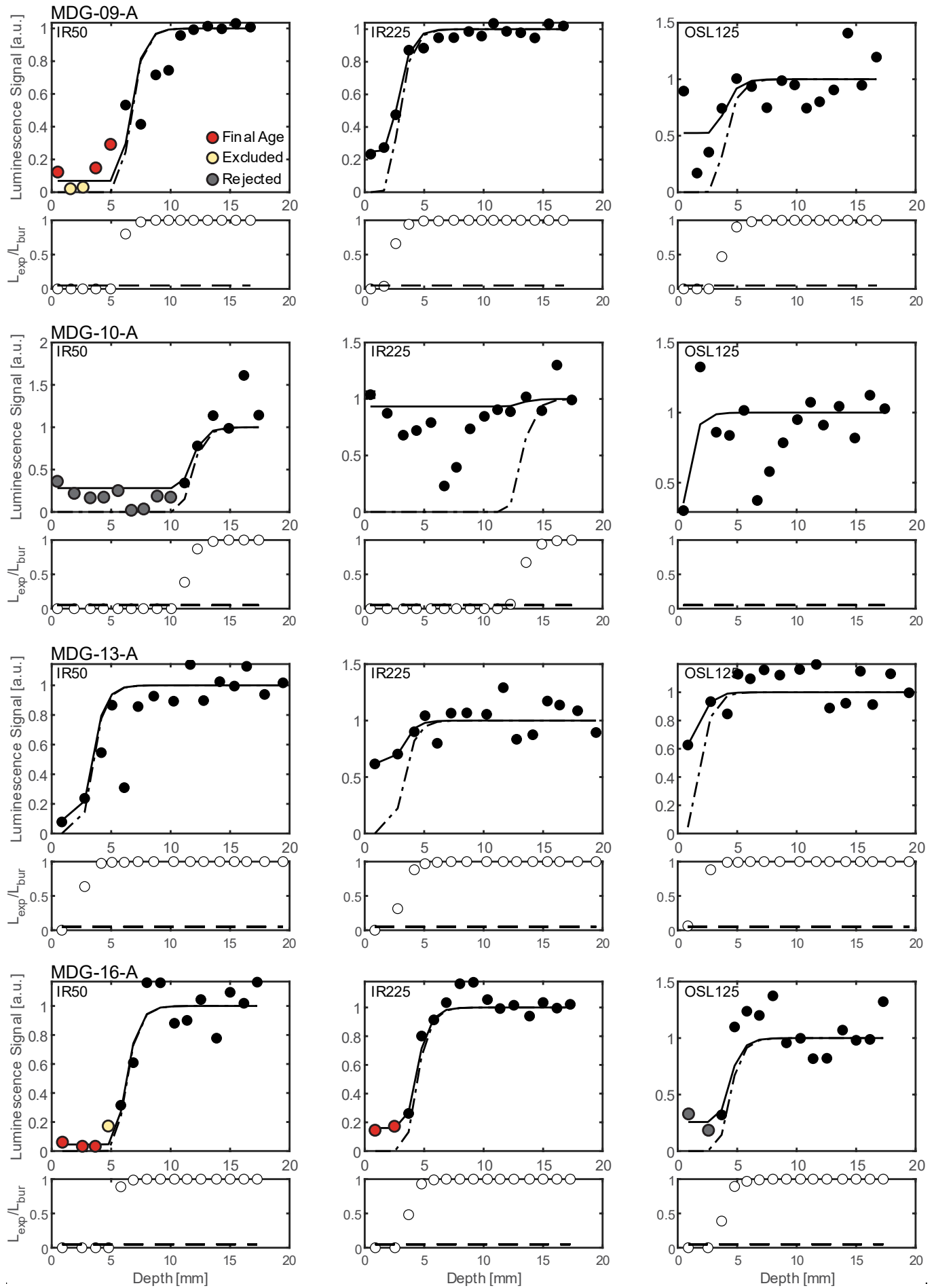


Figure S 24: Luminescence bleaching profiles of RSBD samples: MDG-18 (A), 19 (A), 20 (A,B).

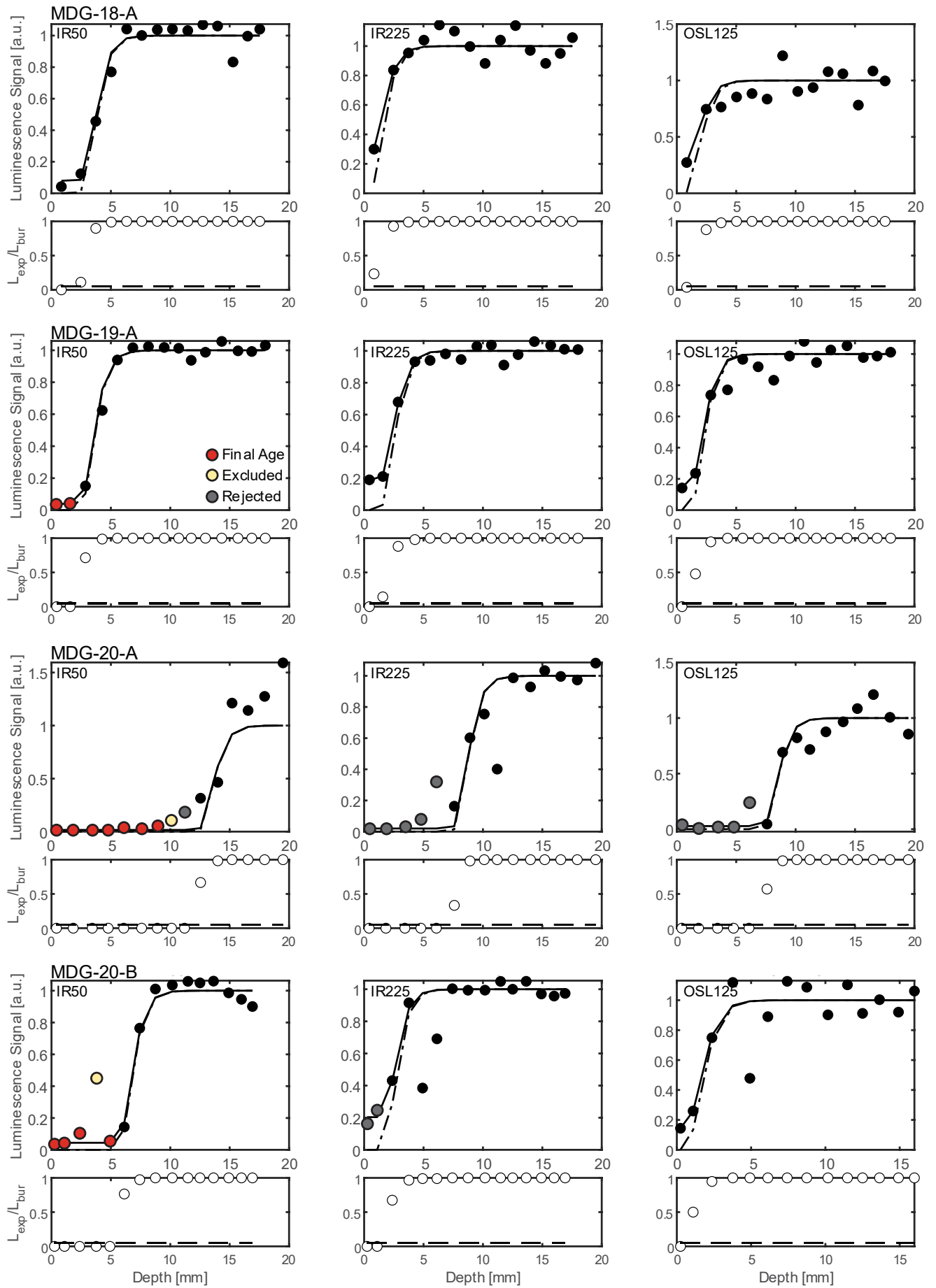


Figure S 25: Luminescence bleaching profiles of RSBD samples: MDG-21 (A), 32 (A), 33 (B).

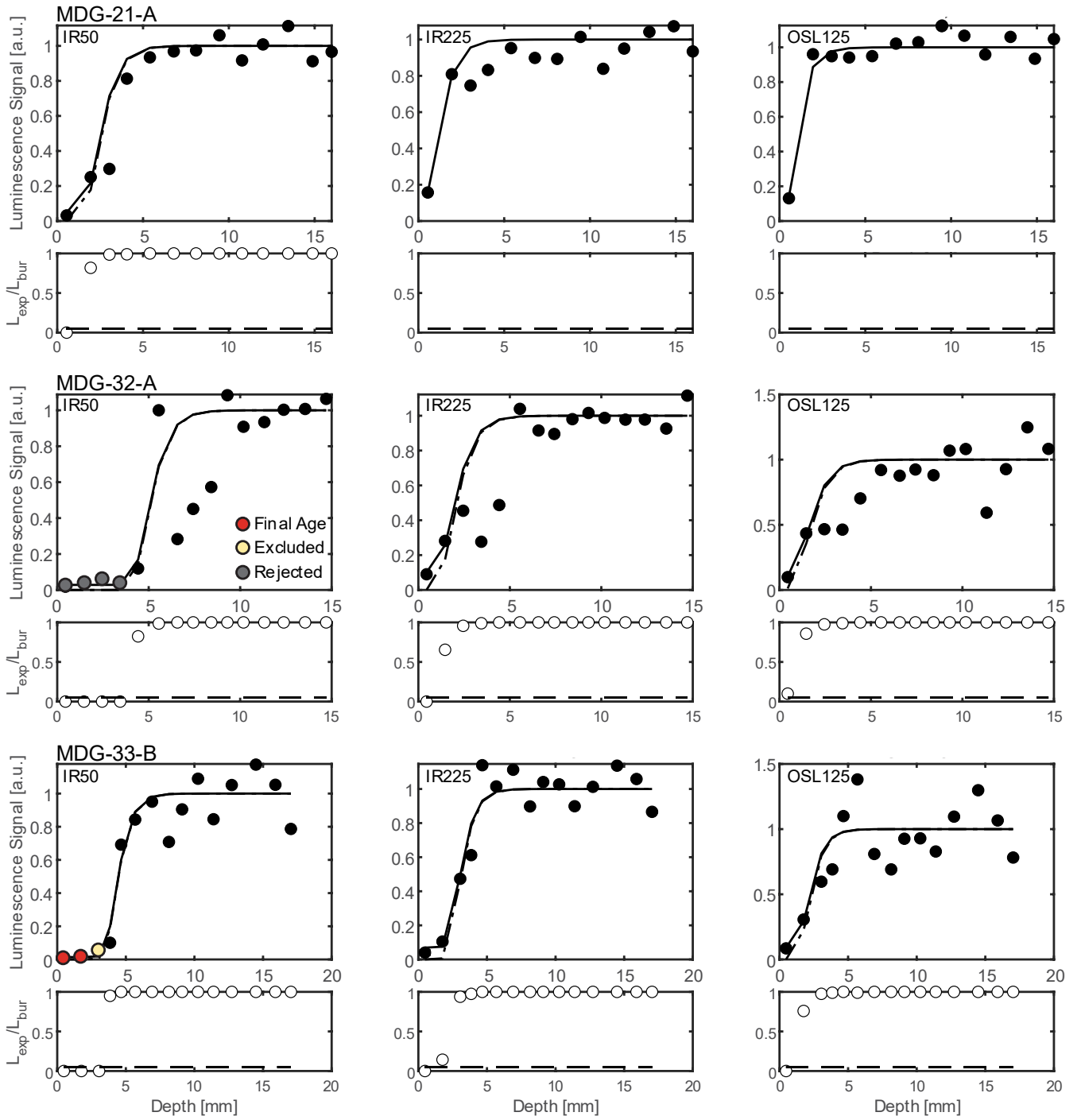


Figure S 26: Dose response curve from sample MDG23_01 core A2 IRSL₅₀ (A), IRSL₂₂₅ (B), and core B2 IRSL₅₀ (C), IRSL₂₂₅ (D)

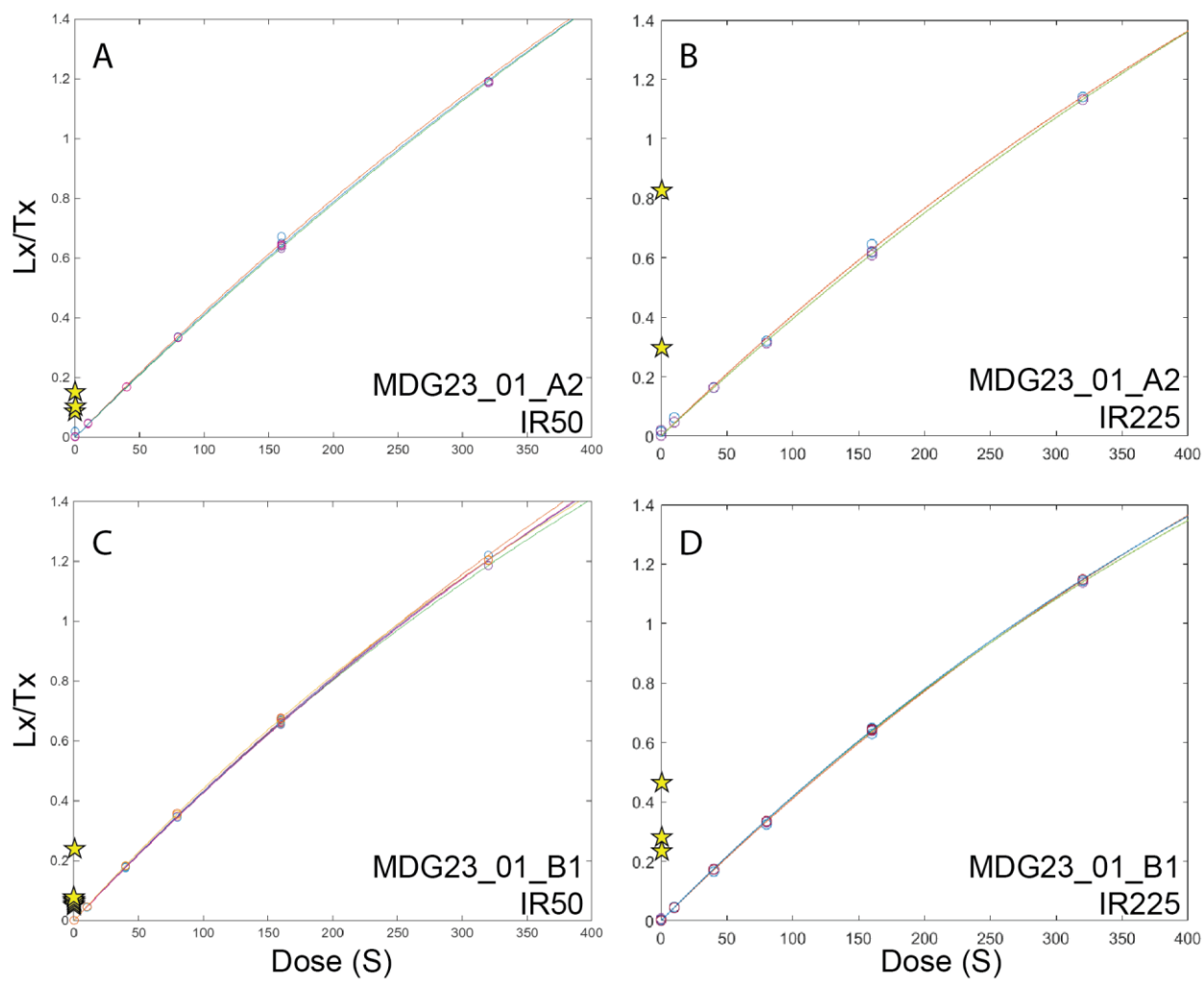


Figure S 27: Dose response curve from sample MDG23_04 core A1 IRSL₅₀ (A), IRSL₂₂₅ (B), and core B1 IRSL₅₀ (C), IRSL₂₂₅ (D)

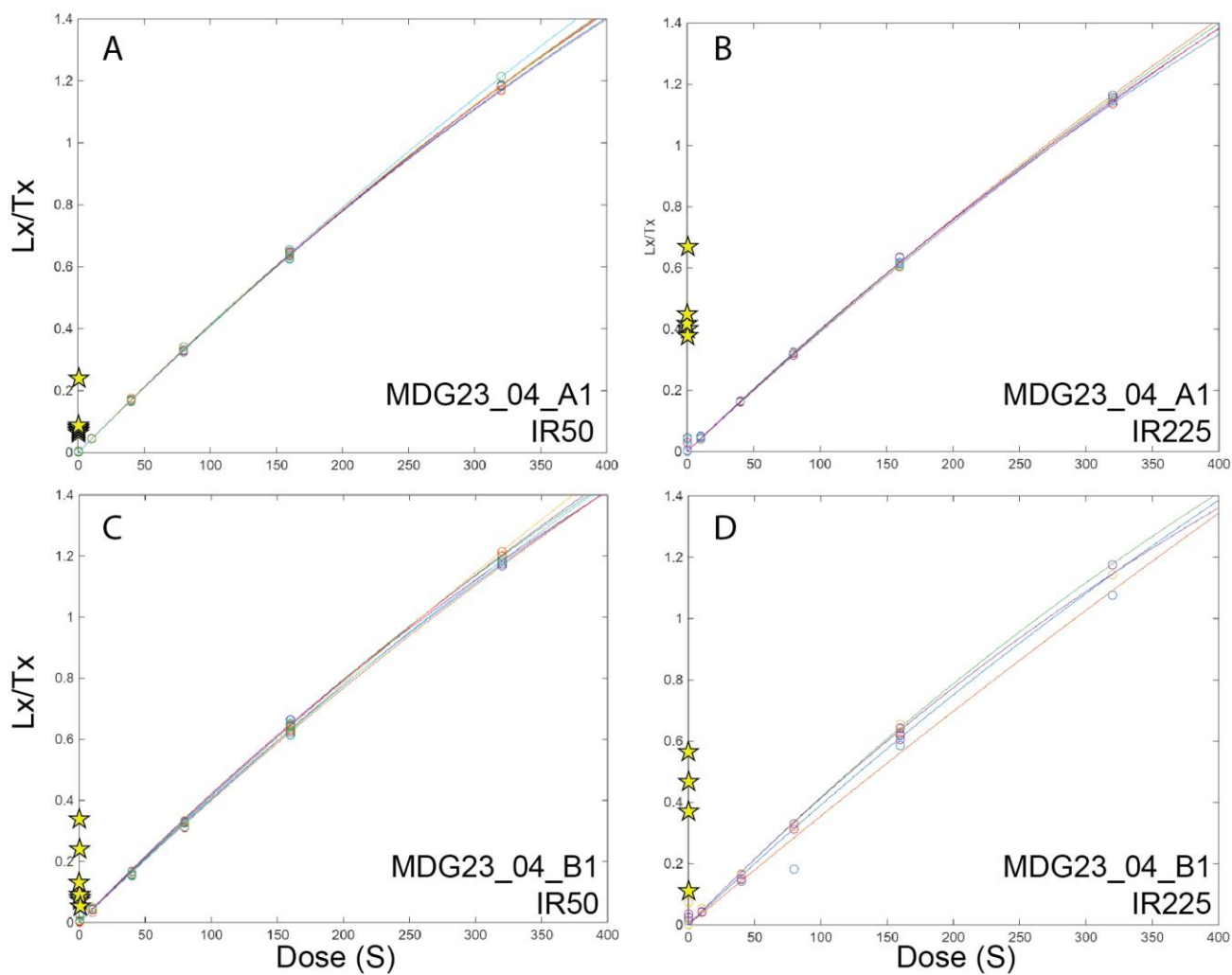


Figure S 28: Dose response curve from sample MDG23_06 core A1 IRSL₅₀

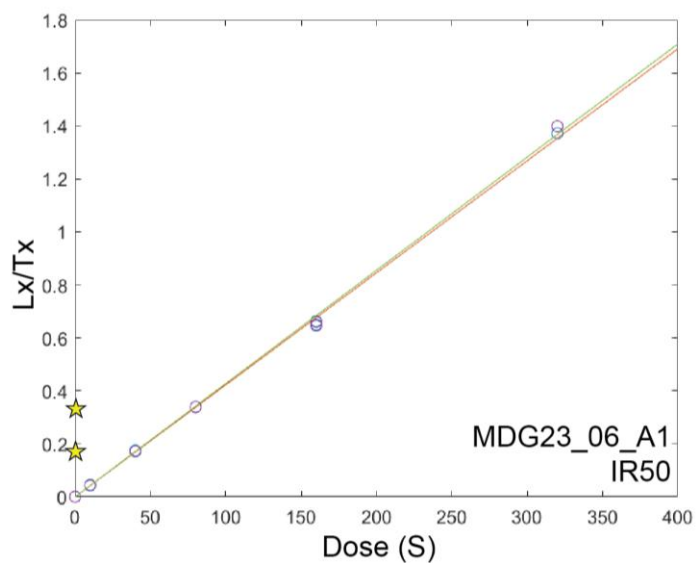


Figure S 29: Dose response curve from sample MDG23_07 core A1 IRSL₅₀ (A), core C1 IRSL₅₀ (B), and core D1 IRSL₅₀ (C)

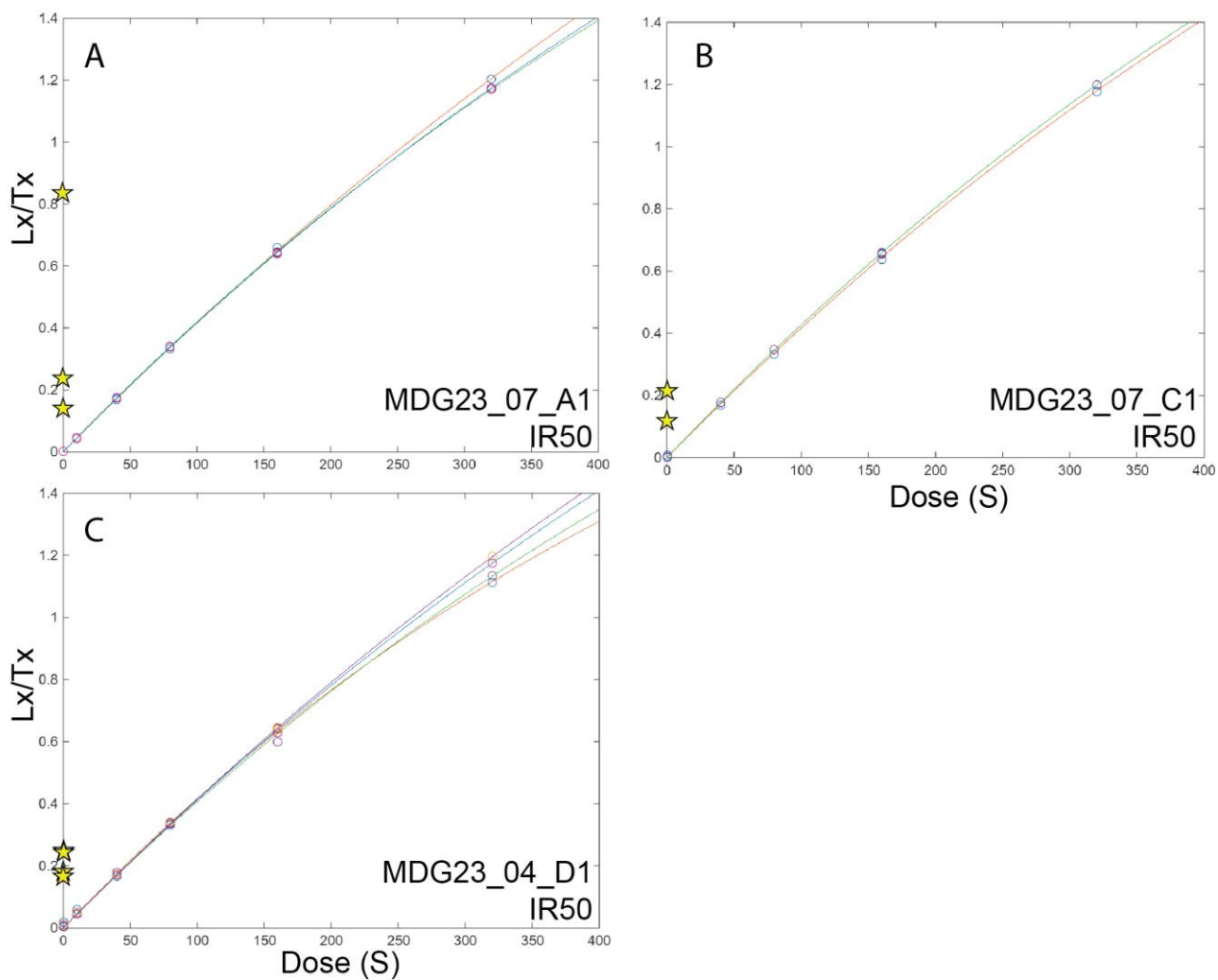


Figure S 30: Dose response curve from sample MDG23_08 core C1 IRSL₅₀

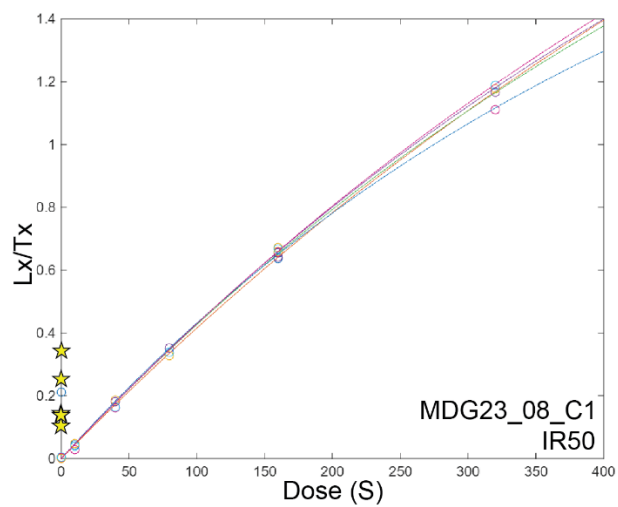


Figure S 31: Dose response curve from sample MDG23_10 core A2 IRSL₅₀ (A), IRSL₂₂₅ (B), and core B2 IRSL₅₀ (C), IRSL₂₂₅ (D)

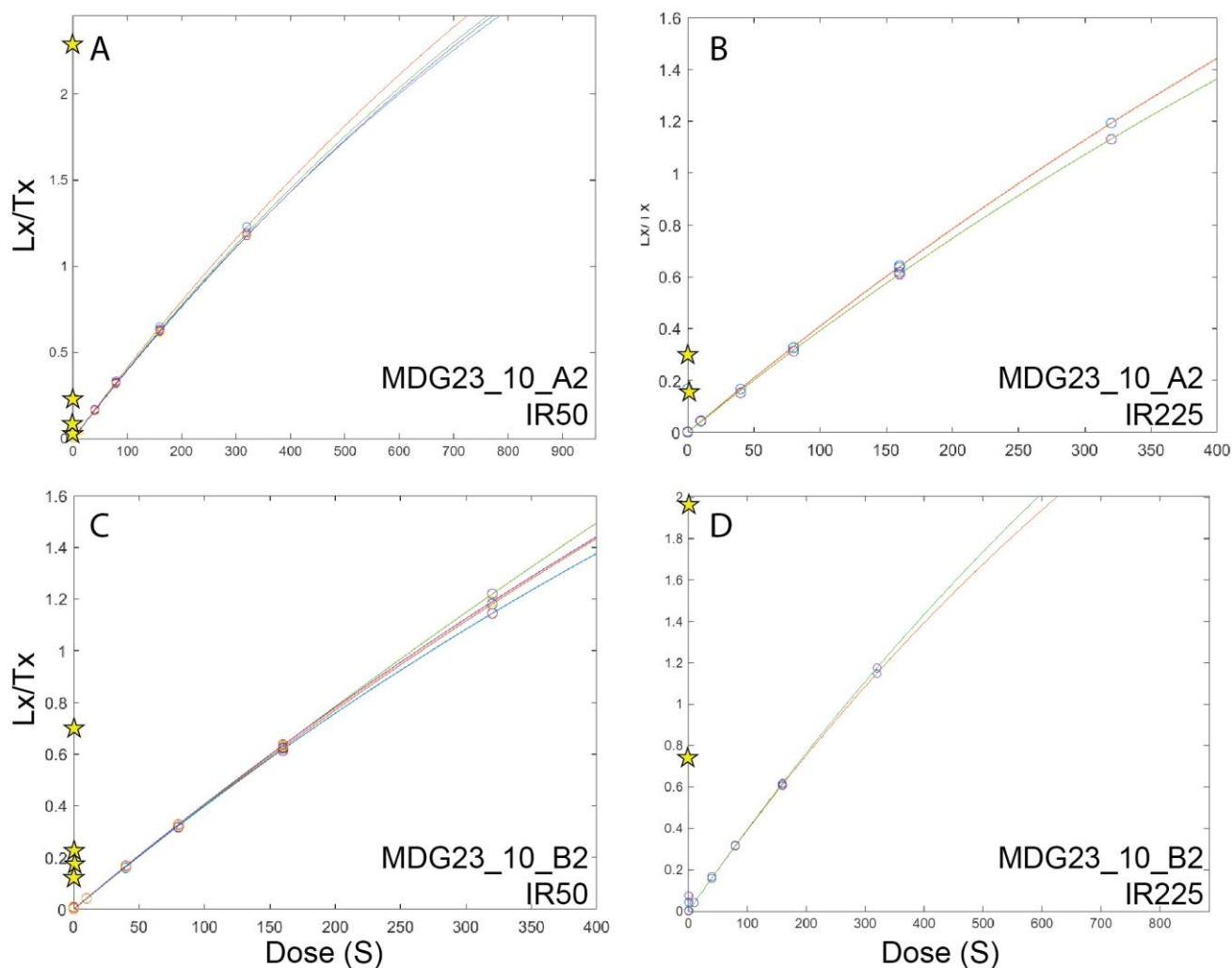


Figure S 32: Dose response curve from sample MDG_01 core A IRSL₅₀

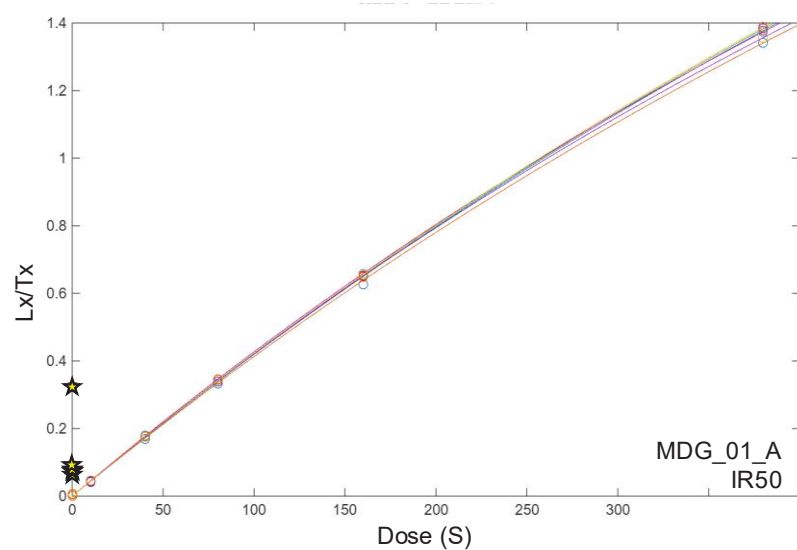


Figure S 33: Dose response curve from sample MDG_02 core B1 IRSL₅₀

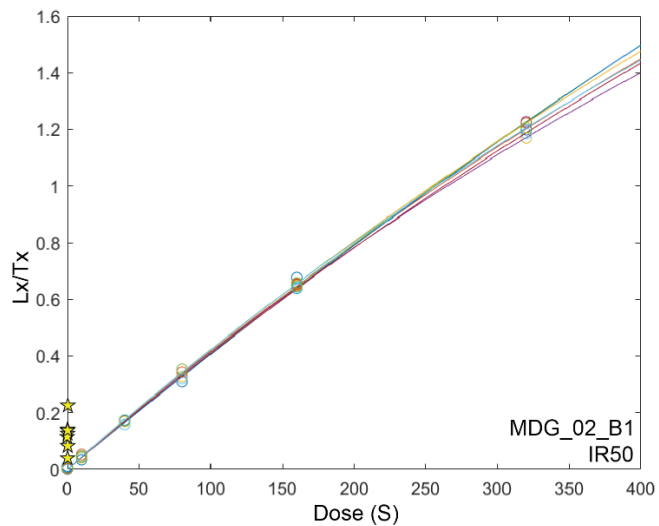


Figure S 34: Dose response curve from sample MDG_06 core A IRSL₅₀

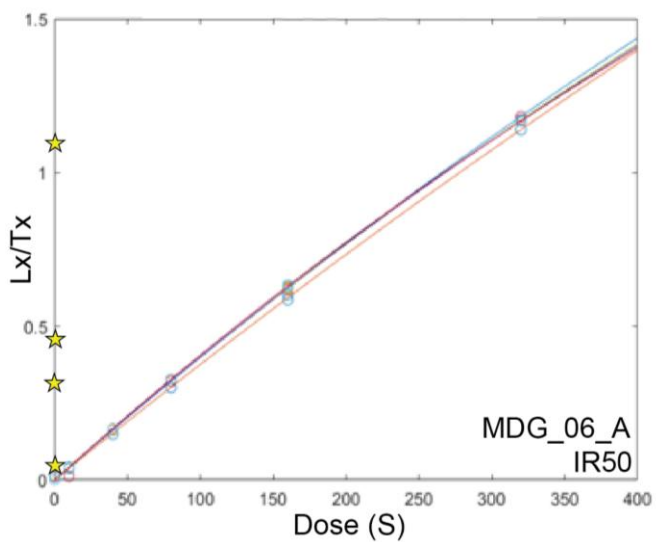


Figure S 35: Dose response curve from sample MDG_07 core A IRSL₅₀

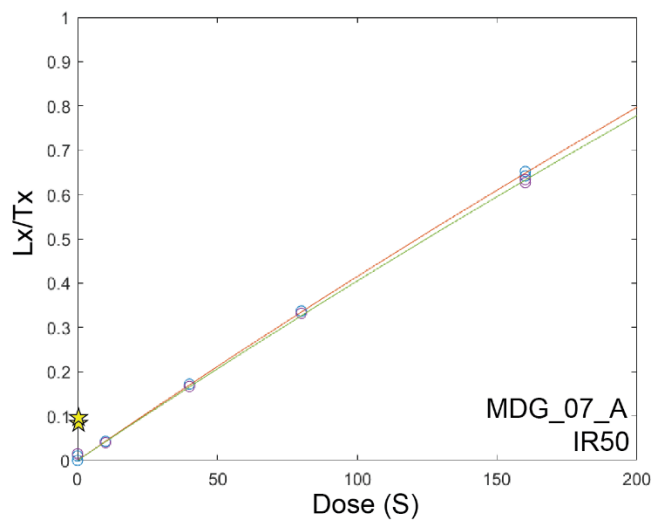


Figure S 36: Dose response curve from sample MDG_09 core A IRSL₅₀

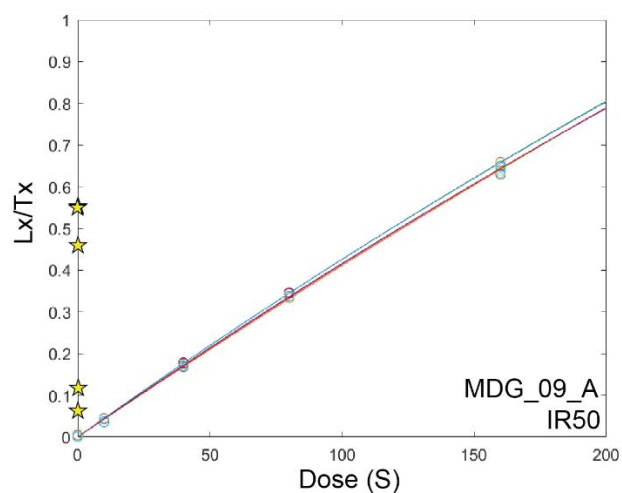


Figure S 37: Dose response curve from sample MDG_16 core A IRSL₅₀ (A), IRSL₂₂₅ (B)

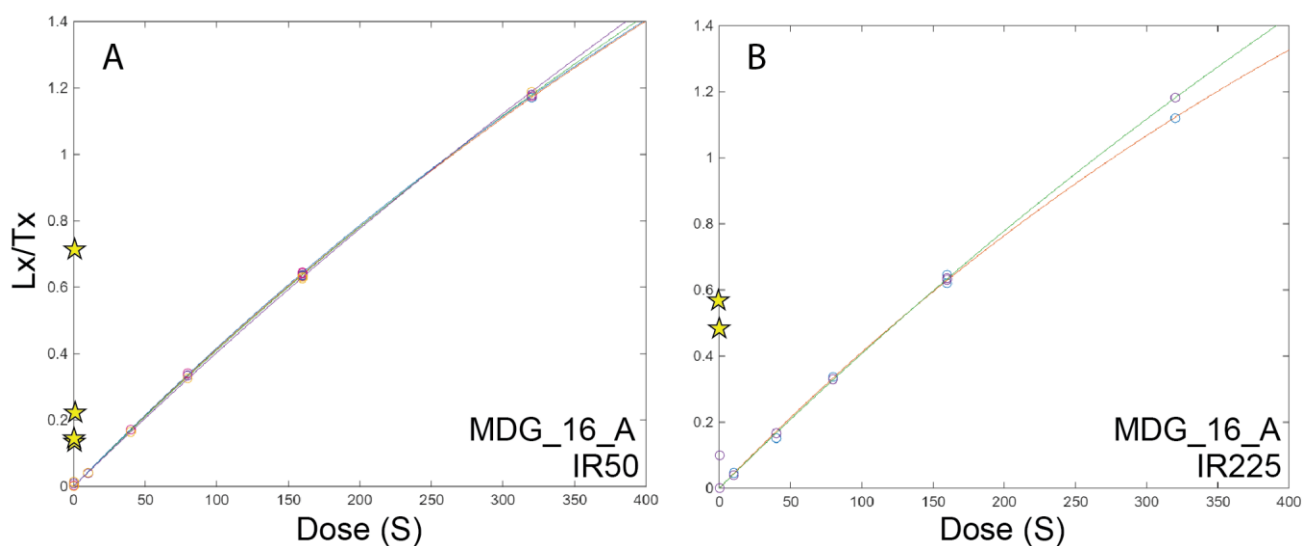


Figure S 38: Dose response curve from sample MDG_19 core A IRSL₅₀

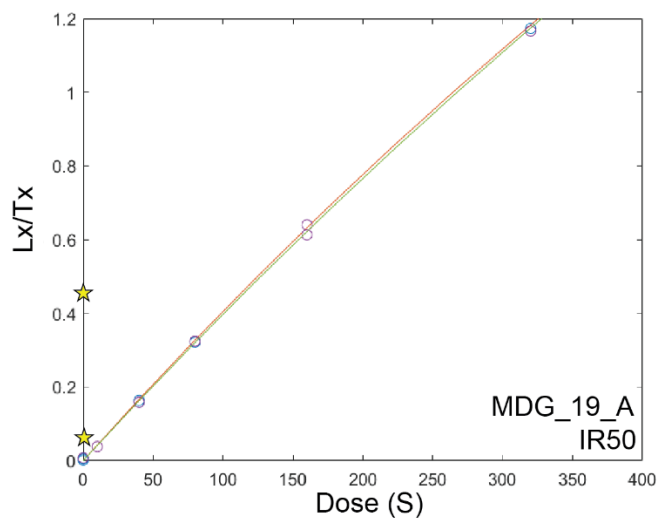


Figure S 39: Dose response curve from sample MDG_20 core A IRSL₅₀ (A), core B IRSL₅₀ (B)

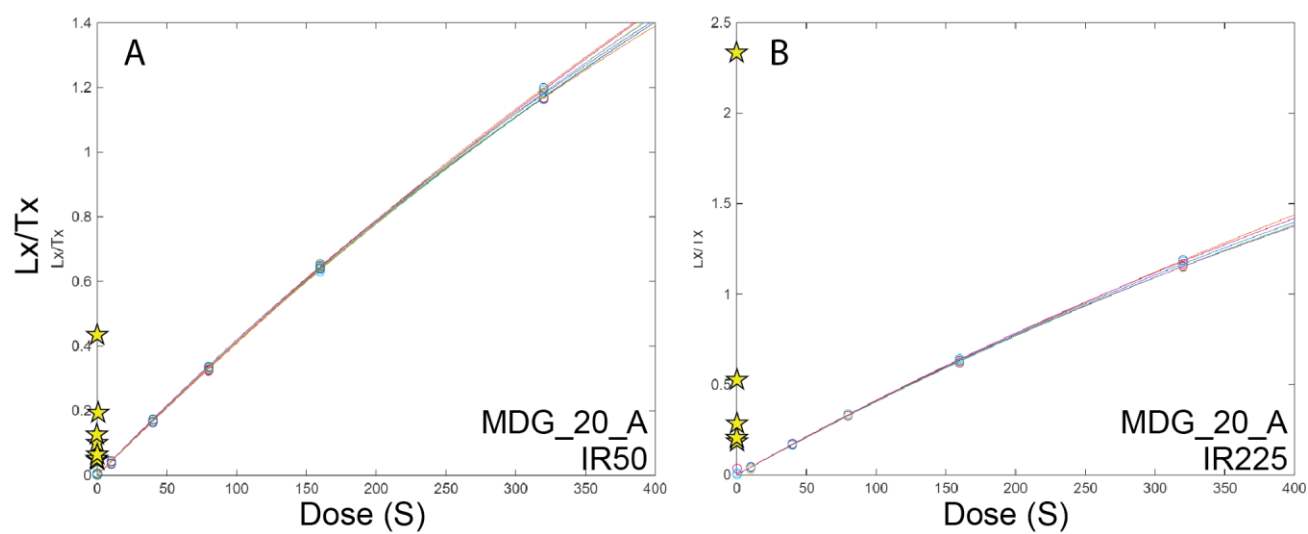


Figure S 40: Dose response curve from sample MDG_33 core A IRSL₅₀

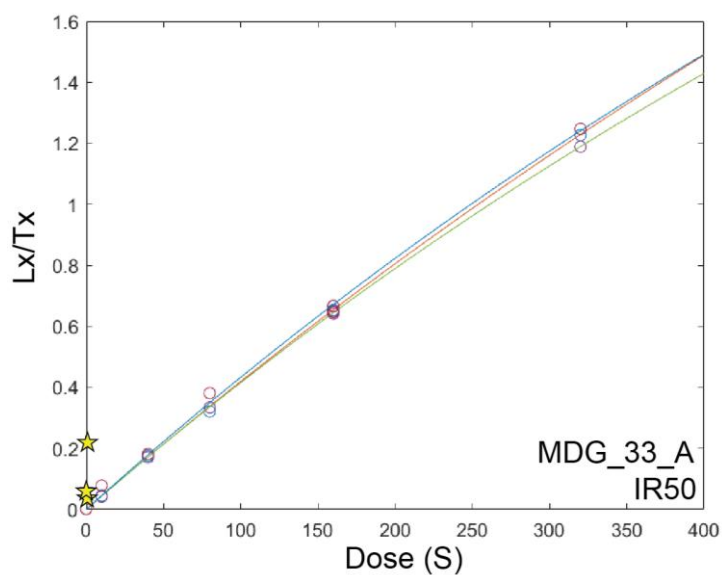


Table S 6: Measured variables for total environmental dose rate (\dot{D}) determination.

Note that the average measured water content of $0.4 \pm 0.4\%$ was used for all samples, as well as an average grain size of $850\text{--}950\text{ }\mu\text{m}$. Radioisotope concentrations of samples MDG23_04, MDG_09 and MDG_19 are based on ICPMS measurements done at Actlabs, Ancaster, Canada.

Sample name	Measured water content [%]	K [%]	Th [ppm]	U [ppm]	Measured grain-size Q [μm]	Measured grain-size F [μm]	Diameter [cm]
MDG23_01	0.18	3.66 ± 0.26	27.3 ± 1.8	7.7 ± 0.5	1040 ± 900 (A2) 990 ± 630 (B2)	1210 ± 1060 (A2) 650 ± 480 (B2)	11
MDG23_04	-	3.96 ± 0.01	27.6 ± 0.1	11.6 ± 0.1	590 ± 370 (A1) 1110 ± 610 (B1)	890 ± 740 (A1) 615 ± 75 (B1)	7
MDG23_06	0.68	3.98 ± 0.28	28.8 ± 1.8	6.7 ± 0.4	750 ± 490	685 ± 455	8
MDG23_07	0.31	3.65 ± 0.27	32.3 ± 1.9	8.0 ± 0.5	750 ± 380 (A1) 990 ± 140 (C1) 695 ± 285 (D1)	955 ± 505 (A1) 1295 ± 675 (C1) 750 ± 280 (D1)	18
MDG23_08	0.18	1.64 ± 0.15	31.3 ± 2.9	11.8 ± 0.8	970 ± 290	910 ± 90	16
MDG23_09	0.39	3.93 ± 0.27	34.9 ± 3.0	13.4 ± 0.9	1750 ± 700	1050 ± 590	10
MDG23_10	0.19	3.46 ± 0.25	44.3 ± 2.9	12.6 ± 0.8	910 ± 570 (A2) 660 ± 130 (B2)	1125 ± 535 (A2) 605 ± 355 (B2)	15
MDG_01	0.22	2.95 ± 0.22	25.9 ± 1.9	8.6 ± 0.5	1355 ± 655	1160 ± 150	8
MDG_02	0.14	3.89 ± 0.27	29.4 ± 2.0	7.1 ± 0.5	1125 ± 195	510 ± 0	15
MDG_03	0.41	2.78 ± 0.21	28.8 ± 2.0	7.1 ± 0.5	1220 ± 580	1290 ± 570	11
MDG_06	0.076	3.28 ± 0.24	31.7 ± 2.4	10.1 ± 0.6	870 ± 310	1120 ± 420	22
MDG_07	0.21	3.44 ± 0.25	31.4 ± 3.1	14.3 ± 0.8	770 ± 80	805 ± 325	13
MDG_09	-	5.06 ± 0.01	38.5 ± 0.1	10.7 ± 0.1	1230 ± 670	1225 ± 665	6
MDG_10	0.18	1.07 ± 0.11	31.0 ± 2.2	7.0 ± 0.6	1320 ± 910	870 ± 270	16
MDG_16	0.35	3.52 ± 0.25	30.8 ± 1.9	8.4 ± 0.4	715 ± 305	1100 ± 730	11
MDG_19	ND	3.52 ± 0.25	30.8 ± 1.9	8.4 ± 0.4	1435 ± 865	2050 ± 220	5
MDG_20	0.73	3.45 ± 0.25	25.9 ± 1.8	7.8 ± 0.4	720 ± 100	1085 ± 575	11
MDG_33	0.11	3.27 ± 0.24	32.2 ± 2.1	8.1 ± 0.6	1310 ± 840	695 ± 165	10

Table S 7: Dose rates, D_e values, luminescence ages calculated per rock fragment for IRSL₅₀

Cores ID and slices	Environm ental dose rate [Gy/Ka]	D _e [Gy]	$\frac{g_{2days}}{[\%decade^{-1}]}$	Uncorrecte d age [ka]	Fading corrected age [ka]	Mean fading corrected age [ka]	Mean fading corrected age excl. rock fragments >1 σ from the mean [ka]
MDG23_01_A2 s1	5.93±0.32	2.93±0.19	5.55±1.07	0.49±0.04	0.63±0.08	0.9±0.26	0.72±0.09
MDG23_01_A2 s2	6.23±0.33	6.00±0.09	5.55±1.07	0.96±0.05	1.25±0.15		
MDG23_01_A2 s3	6.32±0.34	3.92±0.08	5.55±1.07	0.62±0.04	0.8±0.1		
MDG23_01_B1 s1	6.04±0.33	1.74±0.09	5.55±1.07	0.29±0.02	0.37±0.04	0.75±0.53	0.45±0.08
MDG23_01_B1 s2	6.17±0.33	1.87±0.07	5.55±1.07	0.30±0.02	0.39±0.05		
MDG23_01_B1 s3	6.27±0.33	2.72±0.05	5.55±1.07	0.43±0.02	0.56±0.06		
MDG23_01_B1 s4	6.32±0.34	3.16±8.17	5.55±1.07	0.50±1.29	0.65±1145736.8		
MDG23_01_B1 s5	6.36±0.34	2.43±0.08	5.55±1.07	0.38±0.02	0.49±0.5		
MDG23_01_B1 s6	6.40±0.34	8.61±0.05	5.55±1.07	1.35±0.07	1.78±0.21		
MDG23_04_A1 s1	6.15±0.22	3.36±0.59	4.17±0.66	0.55±0.1	0.75±0.15	0.82±0.46	0.64±0.08
MDG23_04_A1 s2	6.44±0.22	2.39±0.15	4.17±0.66	0.37±0.03	0.5±0.05		
MDG23_04_A1 s3	6.51±0.22	2.70±0.32	4.17±0.66	0.42±0.05	0.57±0.08		
MDG23_04_A1 s4	6.56±0.22	3.01±0.24	4.17±0.66	0.46±0.04	0.62±0.07		
MDG23_04_A1 s5	6.58±0.22	3.3±0.22	4.17±0.66	0.5±0.04	0.68±0.07		
MDG23_04_A1 s6	6.6±0.22	3.41±0.19	4.17±0.66	0.52±0.03	0.71±0.06		
MDG23_04_A1 s7	6.6±0.22	9.24±0.65	4.17±0.66	1.40±0.11	1.94±0.2		
MDG23_04_B1 s1	6.34±0.22	2.30±0.53	4.17±0.66	0.36±0.09	0.48±0.13	1.22±0.85	0.94±0.1
MDG23_04_B1 s2	6.48±0.22	2.89±0.31	4.17±0.66	0.45±0.05	0.61±0.08		
MDG23_04_B1 s3	6.54±0.22	3.22±0.19	4.17±0.66	0.49±0.03	0.66±0.06		
MDG23_04_B1 s4	6.58±0.22	3.87±0.22	4.17±0.66	0.59±0.04	0.8±0.08		
MDG23_04_B1 s5	6.59±0.22	4.85±0.43	4.17±0.66	0.74±0.07	1.01±0.12		
MDG23_04_B1 s6	6.6±0.22	9.81±0.73	4.17±0.66	1.49±0.12	2.07±0.23		
MDG23_04_B1 s7	6.61±0.22	13.76±0.68	4.17±0.66	2.08±0.13	2.91±0.28		
MDG23_06_A1 s1¹	5.89±0.31	6.74±1.22	3.01±0.63	1.15±0.22	1.44±0.29		
MDG23_06_A1 s2	6.12±0.33	12.84±221.87	3.01±0.63	2.10±36.27	2.66±30.22		
MDG23_07_A1 s1	6.55±0.34	5.49±0.54	7.27±0.69	0.84±0.09	1.53±0.23	4.92±4.08	2.05±0.52
MDG23_07_A1 s2	6.69±0.35	35.31±0.18	7.27±0.69	5.28±0.28	10.66±1.51		
MDG23_07_A1 s3	6.72±0.35	9.19±0.2	7.27±0.69	1.37±0.08	2.56±0.32		
MDG23_07_C1 s1	6.21±0.32	4.52±0.53	7.27±0.69	0.73±0.09	1.32±0.22	1.8±0.47	1.8±0.47
MDG23_07_C1 s2	0.35±8.12	8.12±0.2	7.27±0.69	1.22±0.07	2.27±0.28		
MDG23_07_D1 s1	6.21±0.32	6.17±0.86	7.27±0.69	1.08±0.15	2.0±0.36	2.37±0.47	2.38±0.38
MDG23_07_D1 s2	6.5±0.34	9.99±1.38	7.27±0.69	1.54±0.23	2.9±0.56		
MDG23_07_D1 s3	6.63±0.34	6.55±0.68	7.27±0.69	0.99±0.12	1.82±0.3		
MDG23_07_D1 s4	6.73±0.35	9.88±0.85	7.27±0.69	1.47±0.15	2.76±0.42		

MDG23_08_C1 s1	5.46±6.84	5.46±6.84	3.19±1.06	0.91±1.14	1.15±17853842	1.62±0.76	1.51±0.49
					8		
MDG23_08_C1 s2	9.5±0.37	9.5±0.37	3.19±1.06	1.56±0.11	2±0.35		
MDG23_08_C1 s3	12.83±0.77	12.83±0.77	3.19±1.06	2.09±0.18	2.69±0.49		
MDG23_08_C1 s4	5.01±1.08	5.01±1.08	3.19±1.06	0.81±0.18	1.02±0.28		
MDG23_08_C1 s5	3.84±0.74	3.84±0.74	3.19±1.06	0.62±0.12	0.78±0.19		
MDG23_10_A2 s1	7.33±0.39	1.42±0.38	5.07±0.29	0.19±0.05	0.28±0.08	6.87±10.28	0.95±0.73
MDG23_10_A2 s2	7.47±0.41	3.12±0.12	5.07±0.29	0.42±0.03	0.61±0.05		
MDG23_10_A2 s3	7.53±0.41	9.82±0.18	5.07±0.29	1.31±0.07	1.96±0.13		
MDG23_10_A2 s4	7.64±0.42	115.91±0.22	5.07±0.29	15.18±0.83	24.63±1.72		
MDG23_10_B2 s1	6.62±0.35	4.80±0.62	5.07±0.29	0.73±0.1	1.07±0.16	2.64±1.02	2.13±0.71
MDG23_10_B2 s2	7.15±0.38	9.45±0.9	5.07±0.29	1.32±0.14	1.98±0.23		
MDG23_10_B2 s3	7.33±0.39	7.08±0.47	5.07±0.29	0.97±0.08	1.44±0.13		
MDG23_10_B2 s4	7.45±0.41	29.07±0.44	5.07±0.29	3.90±0.22	6.06±0.41		
MDG_01A s1	5.81±0.31	12.93±1.10	3.72±0.25	2.23±0.22	3.00±0.33	1.06±0.87	0.67±0.09
MDG_01A s2	5.90±0.32	3.38±0.52	3.72±0.25	0.57±0.09	0.75±0.13		
MDG_01A s3	5.93±0.32	3.68±0.61	3.72±0.25	0.46±0.11	0.60±0.15		
MDG_01A s4	5.95±0.32	2.72±0.63	3.72±0.25	0.62±0.09	0.81±0.13		
MDG_01A s5	5.96±0.32	2.64±0.43	3.72±0.25	0.44±0.08	0.61±0.04		
MDG_01A s6	5.97±0.32	3.04±0.55	3.72±0.25	0.51±0.10	0.58±0.10		
MDG_02B1 s1	6.26±0.34	3.18±1.03	4.58±1.76	0.51±0.17	0.71±0.3	0.94±0.45	0.88±0.17
MDG_02B1 s2	6.56±0.35	1.59±0.31	4.58±1.76	0.24±0.05	0.33±0.09		
MDG_02B1 s3	6.67±0.36	3.11±0.5	4.58±1.76	0.47±0.08	0.66±0.18		
MDG_02B1 s4	6.73±0.36	4.89±0.28	4.58±1.76	0.73±0.06	1.03±0.23		
MDG_02B1 s5	6.80±0.36	8.86±0.44	4.58±1.76	1.30±0.1	1.87±0.44		
MDG_02B1 s6	6.82±0.37	4.33±0.39	4.58±1.76	0.64±0.07	0.9±0.211		
MDG_02B1 s7	6.83±0.37	5.22±0.35	4.58±1.76	0.76±0.07	1.08±0.25		
MDG_06A s1	1.03±2.35	1.87±0.46	3.99±0.62	1.82±4.16	2.50±4.08	12.82±8.64	6.73±0.72
MDG_06A s2	2.51±2.51	12.69±0.21	3.99±0.62	6.58±8.57	9.30±9.48		
MDG_06A s3	2.76±42.59	47.78±0.59	3.99±0.62	17.29±16.12	25.02±19.94		
MDG_06A s4	3.55±2.65	18.54±0.27	3.99±0.62	5.29±3.95	7.45±4.98		
MDG_06A s5	4.33±2.70	18.54±0.19	3.99±0.62	4.29±2.68	6.01±3.49		
MDG_07A s1	6.92±0.41	3.27±0.37	6.73±1.25	0.47±0.06	0.79±0.18	0.85±0.06	0.85±0.06
MDG_07A s2	7.09±0.42	3.82±0.51	6.73±1.25	0.54±0.08	0.91±0.21		
MDG_09A s1	6.84±0.23	18.38±3.12	7.76±1.4	2.69±0.46	5.54±2.06	4.3±2.6	6.13±0.42
MDG_09A s2	7.03±0.23	2.37±0.51	7.76±1.4	0.34±0.07	0.61±0.19		
MDG_09A s3	7.07±0.23	4.25±0.6	7.76±1.4	0.6±0.09	1.13±0.31		
MDG_09A s4	7.09±0.23	21.91±2.22	7.76±1.4	3.09±0.33	6.43±2.18		
MDG_09A s5	7.09±0.23	21.95±1.03	7.76±1.4	3.1±0.18	6.44±2.1		
MDG_16A s1	6.32±0.32	8.66±0.46	4.75±1.87	1.37±0.1	2±0.52	2.84±2.39	1.47±0.37
MDG_16A s2	6.45±0.32	5.28±0.7	4.75±1.87	0.82±0.12	1.18±0.33		
MDG_16A s3	6.49±0.32	5.55±0.37	4.75±1.87	0.86±0.7	1.24±0.32		

MDG_16A s4	6.52±0.33	29.95±1.12	4.75±1.87	4.59±0.29	6.94±2.19		
MDG_19A s1	6.86±0.27	18.50±0.86	4.5±0.89	2.77±0.17	4.03±0.49	2.27±1.76	
MDG_19A s2	6.86±0.27	2.55±1.15	4.5±0.89	0.37±0.17	0.51±0.24		
MDG_20A s1	5.92±0.31	1.95±0.21	2.93±0.23	0.33±0.04	0.4±0.05	1.05±0.96	0.71±0.39
MDG_20A s2	6.19±0.32	1.82±0.22	2.93±0.23	0.29±0.04	0.35±0.05		
MDG_20A s3	6.27±0.33	1.95±0.15	2.93±0.23	0.31±0.03	0.38±0.04		
MDG_20A s4	6.3±0.33	2.78±0.09	2.93±0.23	0.44±0.03	0.54±0.04		
MDG_20A s5	6.32±0.33	5.19±0.17	2.93±0.23	0.82±0.05	1.02±0.07		
MDG_20A s6	6.33±0.33	4.07±0.09	2.93±0.23	0.64±0.04	0.79±0.05		
MDG_20A s7	6.33±0.33	7.47±0.13	2.93±0.23	1.18±0.07	1.47±0.09		
MDG_20A s8	6.33±0.33	17.12±0.14	2.93±0.23	2.70±0.14	3.41±0.2		
MDG_20B s1	5.75±0.3	7.35±0.24	2.93±0.23	1.28±0.08	1.6±0.11	7.99±11.03	2.5±1.1
MDG_20B s2	5.75±0.3	8.26±0.57	2.93±0.23	1.44±0.13	1.8±0.17		
MDG_20B s3	6.22±0.32	21.47±1.83	2.93±0.23	3.45±0.35	4.37±0.46		
MDG_20B s4	6.27±0.33	143.80±1.07	2.93±0.23	22.95±1.21	29.96±1.79		
MDG_20B s5	6.30±0.33	11.22±0.49	2.93±0.23	1.78±0.12	2.23±0.16		
MDG_33A s1	6.02±0.33	1.28±0.24	9.03±0.13	0.21±0.04	0.42±0.09	1.42±1.12	0.8±0.63
MDG_33A s2	6.24±0.34	2.49±0.08	9.03±0.13	0.4±0.03	0.84±0.07		
MDG_33A s3	6.32±0.34	8.22±0.46	9.03±0.13	1.3±0.1	2.99±0.27		

¹youngest slice has been considered for the final age.

Table S 8: Dose rates, D_e values, luminescence ages calculated per rock fragment for IRSL₂₂₅

Cores ID and slices	Environmental dose rate [Gy/Ka]	D _e [Gy]	g _{2days} [%decade ⁻¹]	Uncorrected age [ka]	Fading corrected age [ka]	Mean fading corrected age [ka]	Mean fading corrected age excl. rock fragments >1σ from the mean [ka]
MDG23_01_A2 s1 ¹	5.93±0.32	11.83±2.38	0.65±0.92 ²	1.99±0.42	-	3.94±1.95	
MDG23_01_A2 s2	6.23±0.33	36.67±2.02	0.65±0.92 ²	5.89±0.45	-		
MDG23_01_B1 s1	6.04±0.33	9.09±1.02	0.65±0.92 ²	1.51±0.19	-	2.05±0.6	1.63±0.13
MDG23_01_B1 s2	6.17±0.33	10.84±0.55	0.65±0.92 ²	1.76±0.13	-		
MDG23_01_B1 s3	6.27±0.33	18.12±0.37	0.65±0.92 ²	2.89±0.16	-		
MDG23_04_A1 s1	6.15±0.22	16.57±8.10	1.98±0.18	2.69±1.32	3.14±1.47	3.53±0.81	3.14±0.2
MDG23_04_A1 s2	6.44±0.22	18.83±6.06	1.98±0.18	2.93±0.95	3.42±1.11		
MDG23_04_A1 s3	6.51±0.22	28.35±4.31	1.98±0.18	4.36±0.68	5.11±0.82		
MDG23_04_A1 s4	6.56±0.22	17.76±6.62	1.98±0.18	2.71±1.01	3.16±1.18		
MDG23_04_A1 s5	6.58±0.22	16.07±5.06	1.98±0.18	2.44±0.77	2.84±0.89		
MDG23_04_B1 s1	6.34±0.22	4.92±725.59	1.98±0.18	<i>0.78±114.40</i>	<i>0.9±83.82</i>	3.42±0.59	
MDG23_04_B1 s2	6.48±0.22	14.69±0.89	1.98±0.18	2.27±0.16	2.64±0.19		
MDG23_04_B1 s3	6.54±0.22	19.79±1.72	1.98±0.18	3.03±0.28	3.54±0.33		
MDG23_04_B1 s4	6.58±0.22	22.98±2.09	1.98±0.18	3.49±0.34	4.08±0.41		
MDG23_10_A2 s1	7.33±0.39	6.15±8.27	2.1±0.64	0.84±1.13	0.98±1.02	1.48±0.5	
MDG23_10_A2 s2	7.47±0.41	12.59±0.66	2.1±0.64	1.69±0.13	1.99±0.19		
MDG23_10_B2 s1 ¹	6.62±0.35	32.24±13.19	2.1±0.64	4.87±2.01	5.79±2.37	10.9±5.1	
MDG23_10_B2 s2	7.15±0.38	95.22±26.82	2.1±0.64	13.31±3.82	16.00±4.85		
MDG_16A s1	6.32±0.32	19.52±4.00	3.6±0.31	3.09±0.65	4.15±0.9	4.52±0.37	
MDG_16A s2	6.45±0.32	23.40±15.12	3.6±0.31	3.63±2.35	4.89±2.88		

¹ The youngest slice has been used for the age calculation

Figure S 41: Dose-recovery ratio, residual-subtracted dose-recovery ratio, residual doses and fading rates

A. Dose-recovery ratio (DRR), B. residual-subtracted dose-recovery ratio (RSDRR), C. residual dose, D. fading rates.

DRR, RSDRR and Residual data are available in Table S72, and Fading in Table S7, S8.

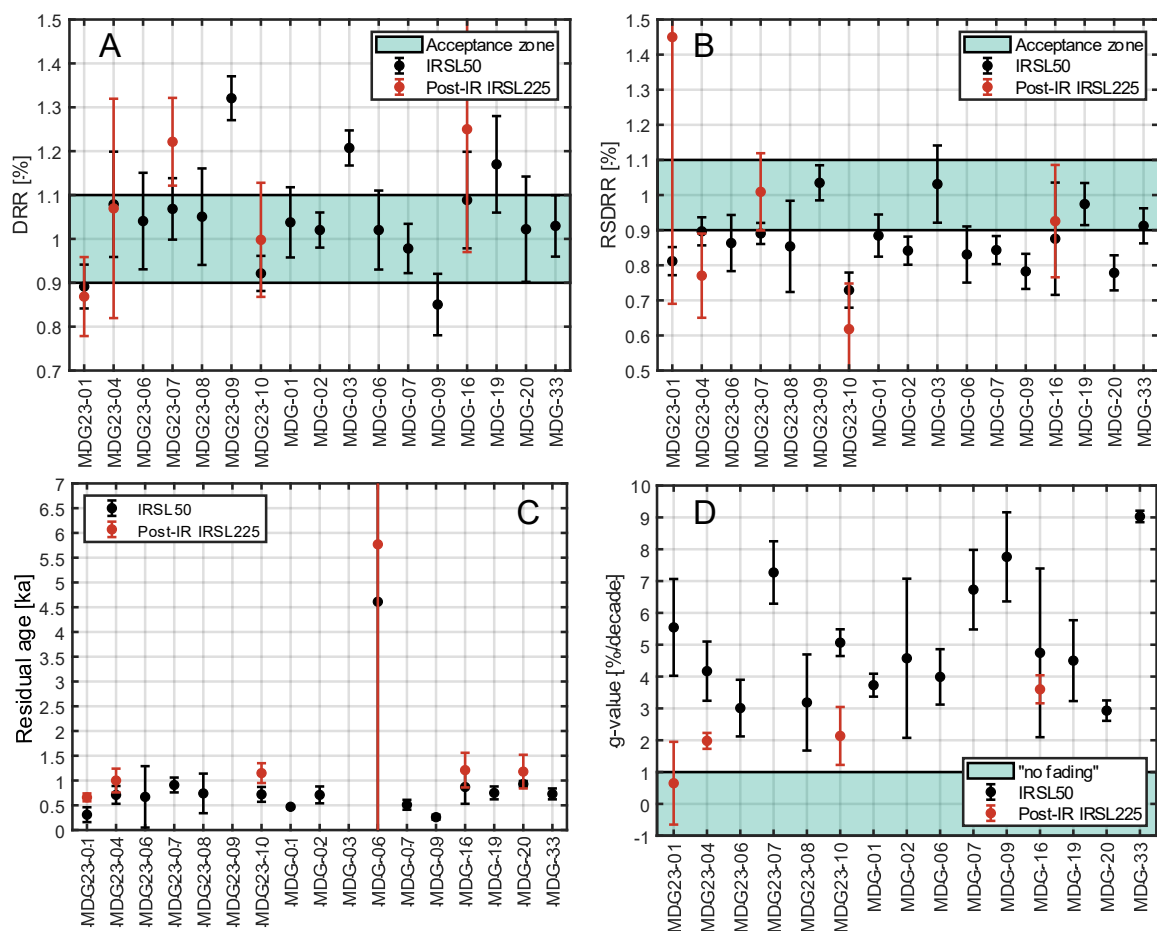


Figure S 42: IRSL₅₀ and IRSL₂₂₅ ages and residuals

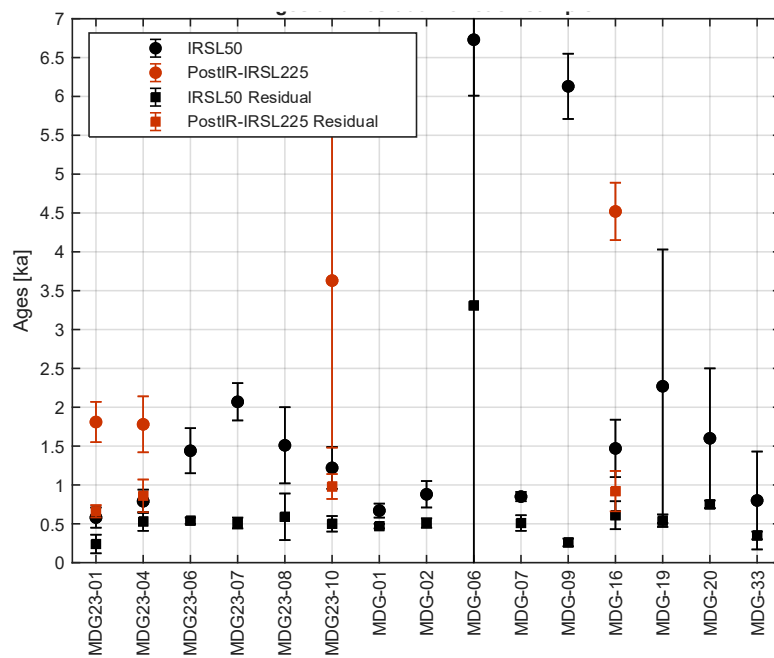


Figure S 43: IRSL₅₀ age variability

Mean fading-corrected IRSL₅₀ ages (red data-points) of all the rock fragment that pass the plateau test per core contrasted with “final” core ages (black data-points) and minimum ages (blue data-points). Final ages are calculated as the mean of the remaining ages after removing those $>1\sigma$ from the mean fading-corrected age. Minimum ages are calculated from the minimum fading-corrected age per core. Numbers indicate the number of aliquots considered for the analysis. Data are available in Table S7.

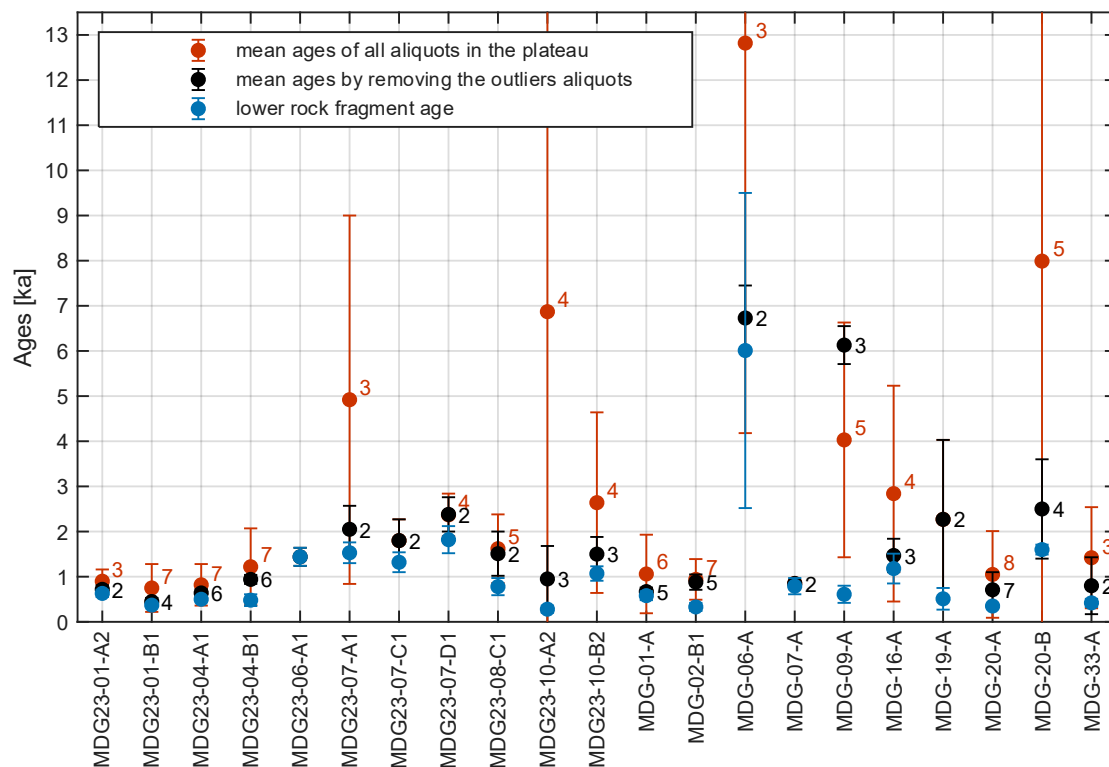


Figure S 44: Distribution of IRSL₅₀ ages by number of rock slice fragments in the plateau

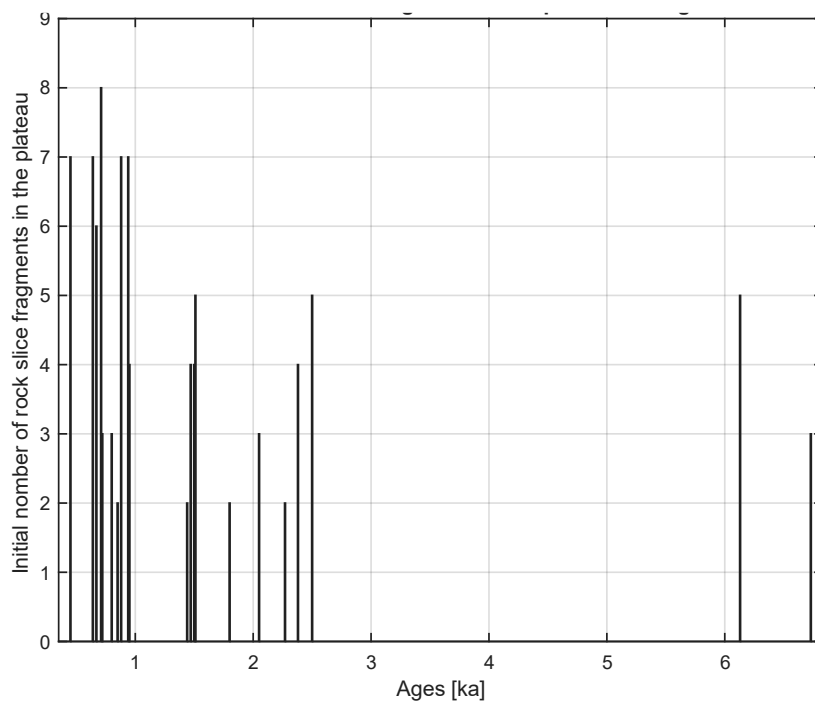
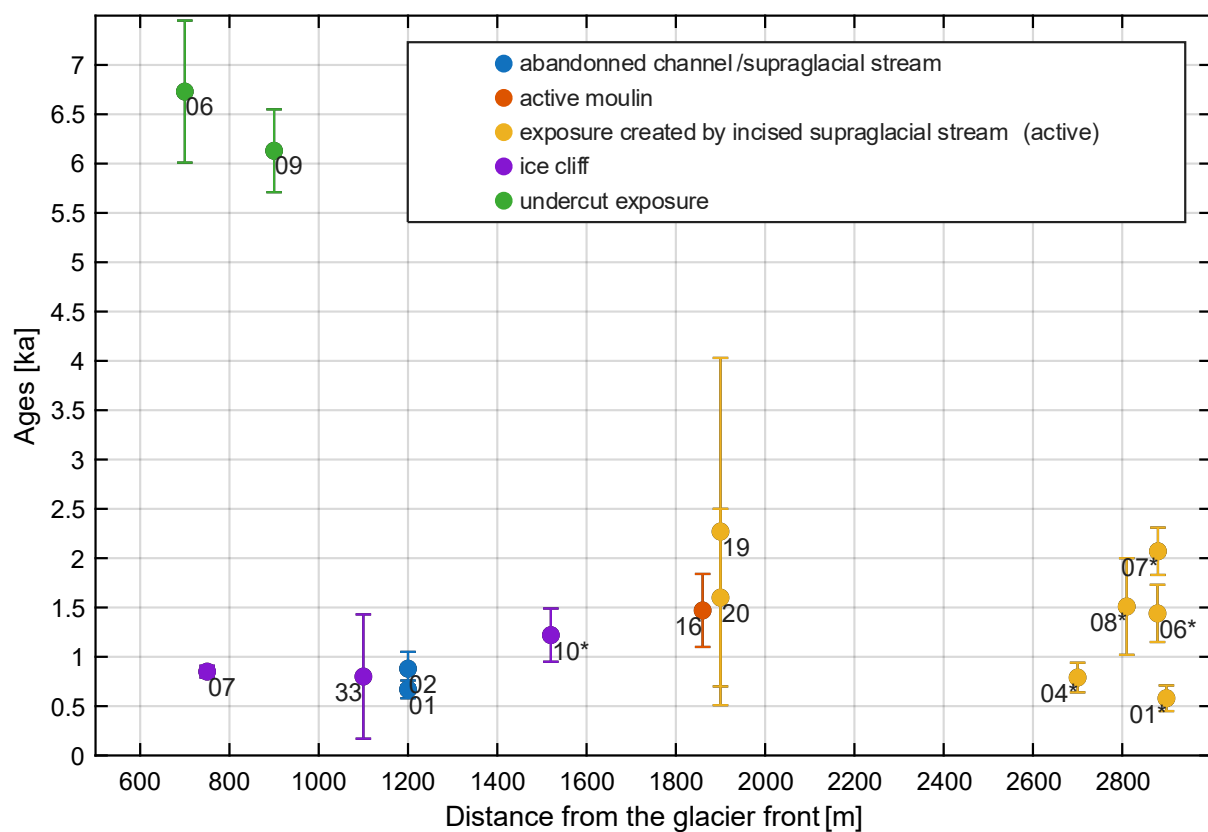


Figure S 45: Ages from the glacier front classified by ice structure



References

- Auclair, M., Lamothe, M., & Huot, S. (2003). Measurement of anomalous fading for feldspar IRSL using SAR. *Radiation Measurements*, 37(4), 487–492. [https://doi.org/10.1016/S1350-4487\(03\)00018-0](https://doi.org/10.1016/S1350-4487(03)00018-0)
- Biswas, R. H., Pathan, A. N., & Malik, J. N. (2023). General order kinetics model for OSL rock surface exposure dating. *Proceedings of the Indian National Science Academy*, 89(3), 644–654. <https://doi.org/10.1007/s43538-023-00172-y>
- Buylaert, J. P., Murray, A. S., Thomsen, K. J., & Jain, M. (2009a). Testing the potential of an elevated temperature IRSL signal from K-feldspar. *Radiation Measurements*, 44(5), 560–565. <https://doi.org/10.1016/j.radmeas.2009.02.007>
- Buylaert, J. P., Murray, A. S., Thomsen, K. J., & Jain, M. (2009b). Testing the potential of an elevated temperature IRSL signal from K-feldspar. *Radiation Measurements*, 44(5–6), 560–565. <https://doi.org/10.1016/j.radmeas.2009.02.007>
- Colarossi, D., Duller, G. A. T., Roberts, H. M., Tooth, S., & Lyons, R. (2015). Comparison of paired quartz OSL and feldspar post-IR IRSL dose distributions in poorly bleached fluvial sediments from South Africa. *Quaternary Geochronology*, 30, 233–238. <https://doi.org/10.1016/j.quageo.2015.02.015>
- Freiesleben, T. H., Thomsen, K. J., Sellwood, E., Liu, J., & Murray, A. S. (2023). Testing new kinetic models and calibration methods for Rock Surface Luminescence Exposure dating using controlled experiments. *Radiation Measurements*, 169, 107033. <https://doi.org/10.1016/j.radmeas.2023.107033>
- Freiesleben, T., Sohbat, R., Murray, A., Jain, M., al Khasawneh, S., Hvidt, S., & Jakobsen, B. (2015). Mathematical model quantifies multiple daylight exposure and burial events for rock surfaces using luminescence dating. *Radiation Measurements*, 81, 16–22. <https://doi.org/10.1016/j.radmeas.2015.02.004>
- Herber, L. (1969). Separation of feldspar from quartz by flotation. *The American Mineralogist*, 54, 1212–1216.
- Huntley, D. J., & Lamothe, M. (2001). Ubiquity of anomalous fading in K-feldspars and the measurement and correction for it in optical dating. *Canadian Journal of Earth Sciences*, 38(7), 1093–1106. <https://doi.org/10.1139/e01-013>
- Kreutzer, S., Burow, C., Dietze, M., Fuchs, M. C., Fischer, M., & Schmidt, C. (2017). Software in the context of luminescence dating: Status, concepts and suggestions exemplified by the R package 'Luminescence'. *Ancient TL*, 35(2), 1–11.
- Lehmann, B., Herman, F., Valla, P. G., King, G. E., & Biswas, R. H. (2019). Evaluating post-glacial bedrock erosion and surface exposure duration by coupling in situ optically stimulated luminescence and ¹⁰Be dating. *Earth Surface Dynamics*, 7(3), 633–662. <https://doi.org/10.5194/esurf-7-633-2019>
- Lehmann, B., Herman, F., Valla, P. G., King, G. E., Biswas, R. H., Ivy-Ochs, S., Steinemann, O., & Christl, M. (2019a). Postglacial erosion of bedrock surfaces and deglaciation timing: New insights from the Mont Blanc massif (western Alps). *Geology*, 48(2), 139–144. <https://doi.org/10.1130/G46585.1>
- Lehmann, B., Herman, F., Valla, P. G., King, G. E., Biswas, R. H., Ivy-Ochs, S., Steinemann, O., & Christl, M. (2019b). Postglacial erosion of bedrock surfaces and deglaciation timing: New insights from the Mont Blanc massif (western Alps). *Geology*, 48(2), 139–144. <https://doi.org/10.1130/G46585.1>
- Mendelová, M., Hein, A. S., Rodés, Á., Smedley, R. K., & Xu, S. (2020). Glacier expansion in central Patagonia during the Antarctic Cold Reversal followed by retreat and stabilisation during the Younger Dryas. *Quaternary Science Reviews*, 227, 106047. <https://doi.org/10.1016/j.quascirev.2019.106047>
- Nishiizumi, K., Imamura, M., Caffee, M. W., Southon, J. R., Finkel, R. C., & McAninch, J. (2007). Absolute calibration of ¹⁰Be AMS standards. *Nuclear Instruments and Methods in Physics Research Section B: Beam Interactions with Materials and Atoms*, 258(2), 403–413. <https://doi.org/10.1016/j.nimb.2007.01.297>
- Pathan, A. N., Biswas, R. H., Lehmann, B., King, G. E., & Herman, F. (2024). Towards accurate modelling of rock surface exposure dating using luminescence to estimate post-exposure erosion rate. *Quaternary Geochronology*, 85, 101634. <https://doi.org/10.1016/j.quageo.2024.101634>
- Raup, B., Kääb, A., Kargel, J. S., Bishop, M. P., Hamilton, G., Lee, E., Paul, F., Rau, F., Soltesz, D., Khalsa, S. J. S., Beedle, M., & Helm, C. (2007). Remote sensing and GIS technology in the Global Land Ice Measurements from Space (GLIMS) Project. *Computers & Geosciences*, 33(1), 104–125. <https://doi.org/10.1016/j.cageo.2006.05.015>
- Riedesel, S., & Autzen, M. (2020). Beta and gamma dose rate attenuation in rocks and sediment. *Radiation Measurements*, 133, 106295. <https://doi.org/10.1016/j.radmeas.2020.106295>
- Xu, S., Dougans, A. B., Freeman, S. P. H. T., Schnabel, C., & Wilcken, K. M. (2010). Improved ¹⁰Be and ²⁶Al-AMS with a 5 MV spectrometer. *Nuclear Instruments and Methods in Physics Research Section B: Beam Interactions with Materials and Atoms*, 268(7), 736–738. <https://doi.org/10.1016/j.nimb.2009.10.018>